

(12) LEVEL III

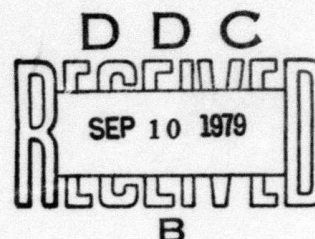
RADC-TR-79-190
Final Technical Report
July 1979



ANALYSIS OF TECHNIQUES FOR IMAGING THROUGH THE ATMOSPHERE

Optical Sciences Company

Sponsored by
Defense Advanced Research Projects Agency (DoD)
ARPA Order No. 2646



APPROVED FOR PUBLIC RELEASE; DISTRIBUTION UNLIMITED

The views and conclusions contained in this document are those of the authors and should not be interpreted as necessarily representing the official policies, either expressed or implied, of the Defense Advanced Research Projects Agency or the U.S. Government.

ROME AIR DEVELOPMENT CENTER
Air Force Systems Command
Griffiss Air Force Base, New York 13441

79 09 10 015

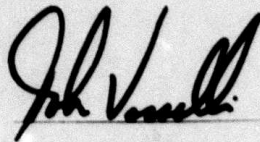
AD A 073 640

DDC FILE COPY

This report has been reviewed by the RADC Information Office (OI) and is releasable to the National Technical Information Service (NTIS). At NTIS it will be releasable to the general public, including foreign nations.

RADC-TR-79-190 has been reviewed and is approved for publication.

APPROVED:



JOHN J. VASSELLI
Project Engineer

If your address has changed or if you wish to be removed from the RADC mailing list, or if the addressee is no longer employed by your organization, please notify RADC (OCSE), Griffiss AFB NY 13441. This will assist us in maintaining a current mailing list.

Do not return this copy. Retain or destroy.

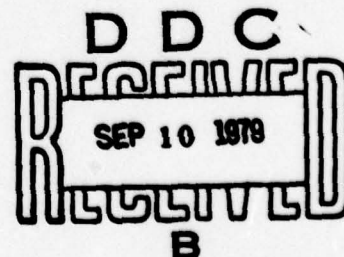
ANALYSIS OF TECHNIQUES FOR IMAGING THROUGH THE ATMOSPHERE

Dr. David L. Fried

Contractor: Optical Sciences Company
Contract Number: F30602-77-C-0021
Effective Date of Contract: 1 Oct 76
Contract Expiration Date: 31 Mar 79
Short Title of Work: Analysis of Techniques for Imaging Through
The Atmosphere
Program Code Number: 9E20
Period of Work Covered: Nov 78 - Apr 79
Principal Investigator: Dr. David Fried
Phone: 714 524-3622
Project Engineer: John J. Vasselli
Phone: 315 330-3144

Approved for public release; distribution unlimited.

This research was supported by the Defense Advanced Research Projects Agency of the Department of Defense and was monitored by John J. Vasselli (OCSE), Griffiss AFB NY 13441 under Contract F30602-77-C-0021.



UNCLASSIFIED

SECURITY CLASSIFICATION OF THIS PAGE (When Data Entered)

REPORT DOCUMENTATION PAGE		READ INSTRUCTIONS BEFORE COMPLETING FORM
1. REPORT NUMBER RADC-TR-79-190	2. GOVT ACCESSION NO.	3. RECIPIENT'S CATALOG NUMBER
4. TITLE (and Subtitle) ANALYSIS OF TECHNIQUES FOR IMAGING THROUGH THE ATMOSPHERE	5. TYPE OF REPORT & PERIOD COVERED Final Technical Report Nov 78 - Apr 79	6. PERFORMING ORG. REPORT NUMBER DR-138
7. AUTHOR(s) Dr. David L. Fried	8. CONTRACT OR GRANT NUMBER(s) F30602-77-C-0021 ✓ ARPA Order-2646	9. PROGRAM ELEMENT, PROJECT, TASK AREA & WORK UNIT NUMBERS 62301E 2646D119
10. PERFORMING ORGANIZATION NAME AND ADDRESS The Optical Sciences Company P.O. Box 446 Placentia CA 92670	11. CONTROLLING OFFICE NAME AND ADDRESS Defense Advanced Research Projects Agency 1400 Wilson Blvd Arlington VA 22209	12. REPORT DATE Jul 1979
13. MONITORING AGENCY NAME & ADDRESS (if different from Controlling Office) Rome Air Development Center (OCSE) Griffiss AFB NY 13441	14. SECURITY CLASS. (of this report) UNCLASSIFIED	15. NUMBER OF PAGES 98
16. DISTRIBUTION STATEMENT (of this Report) Approved for public release; distribution unlimited.		
17. DISTRIBUTION STATEMENT (of the abstract entered in Block 20, if different from Report) Same		
18. SUPPLEMENTARY NOTES RADC Project Engineer: John J. Vasselli (OCSE)		
19. KEY WORDS (Continue on reverse side if necessary and identify by block number) speckle imagery Synthetic Aperture Speckle Imagery Interferometry		
20. ABSTRACT (Continue on reverse side if necessary and identify by block number) This report is concerned with the application of speckle imagery to space object identification for deep space objects. A novel type of variable Michelson Stellar Interferometer setup for forming speckle image data is described. Also, the theory of noise in speckle imagery is developed on a rigorous basis. This report is the final technical report on this contract.		

DD FORM 1 JAN 73 1473

UNCLASSIFIED

SECURITY CLASSIFICATION OF THIS PAGE (When Data Entered)

391 358

JOC

TABLE OF CONTENTS

<u>Section</u>	<u>Title</u>	<u>Page</u>
	Chapter 1 - Report Overview	1
	Chapter 2 - A Speckle Imagery System for Deep Space SOI	4
2.1	Introduction	5
2.2	Basic Considerations	6
2.3	System Description	10
2.4	Base Aperture Unit	13
2.5	Mobile Aperture Unit	15
2.6	Speckle Forming Unit	16
2.7	Operational Procedure	21
2.8	Total Exposure Time	25
2.9	Conclusions	27
2.10	References for Chapter 2	28
	Chapter 3 - Noise in Speckle Interferometry and In Speckle Imagery	29
3.1	Introduction	30
3.2	Averaging Formalism: Turbulence	32
3.3	Averaging Formalism: Photon Detection	37
3.4	Averaging Formalism: Photon Detection and Wavefront Distortion	43
3.5	Spatial Frequency Spectral Moments: Photon Detection Averaging	44
3.6	Unbiased Speckle Measurement Quantities	52
3.7	Speckle Interferometry Measurement Accuracy	56
3.8	Averaging Over Turbulence	60
3.9	Speckle Interferometry Measurement Accuracy	63
3.10	Accuracy of Speckle Imagery	75
3.11	Speckle Imagery Phase Difference Error	77
3.12	Speckle Imagery Resolution	83
3.13	References for Chapter 3	89

LIST OF FIGURES

<u>Figure No.</u>	<u>Title</u>	<u>Page</u>
1	Nominal Form of Michelson Stellar Interferometer	7
2	Overview of Synthetic Aperture Speckle Imagery System	13
3	Optical Block Diagram for Base Aperture Unit	15
4	Speckle Forming Unit Positioning Considerations	17
5	Optical Path Expander	18
6	White Light Interferometer Optical Layout	18
7	Optical Layout of the Speckle Forming Unit	22

ACCESSION for		
NTIS	White Section	<input checked="" type="checkbox"/>
DDC	Diff Section	<input type="checkbox"/>
UNCLASSIFIED		<input type="checkbox"/>
1. CITATION		
BY		
DISTRIBUTION/AVAILABILITY CODES		
Dist. <input type="checkbox"/> <input type="checkbox"/> <input type="checkbox"/> or SPECIAL		
A		

Chapter 1

Report Overview

This report is concerned with the application of speckle imagery techniques to the task of space object identification for deep space objects. It is easy to see that because of the very large range involved, a ground-based imaging system would have to have a diameter of the order of 100 m to provide really useful resolution. The almost certainly impossible nature of a conventional adaptive optics system of this size forces us to seek other approaches to the imaging problem. The approach we investigate in this report is based on a Michelson interferometer version of a speckle imaging system.

The technical content of this report is set forth in two chapters. The first of these, Chapter 2, provides a moderately detailed description of the Michelson Interferometer version of the speckle imaging system. The system described consists of three units: a stationery 4 m diameter telescope, a mobile 1 m diameter telescope, and a mobile speckle-forming unit, along with a flat concrete "apron", semi-circular in shape and with a 100 m radius. During an extended "exposure period" of tens of minutes to several hours, the mobile telescope moves about the apron, and together with the stationary telescope, provides optical inputs to the speckle-forming unit, based on which a series of speckle images are formed and recorded. After the "exposure period," the set of recorded speckle images are processed and a high resolution image of the object in question is developed. Chapter 2 describes the critical features of each unit, and the system's mode of operation.

In Chapter 3, the problem of noise in speckle imagery and speckle interferometry is addressed. A rigorous analytic basis is developed and formulas are obtained for the rms error in speckle imagery as a function of such things as target size, target brightness, and number of exposures. Sample results particularized to a full circular aperture are presented.

These will be generalized to a Michelson interferometer type aperture at a later time. For the case of the circular aperture, in Eq. (3.161) a simple expression is given for the required target brightness so that speckle imagery results will not be limited by photon shot noise, but rather by the limited number of short exposure samples.

Chapter 2

A Speckle Imagery System

for

Deep Space SOI

2.1 Introduction

Space object identification (SOI) of deep space objects by formation of a visible light image, from a ground station, poses a number of major problems. The two most demanding considerations derive from the problem of imaging through atmospheric turbulence and from simple, λ/D - type diffraction considerations. For deep space SOI we are, of necessity, forced to consider aperture diameters of the order of 10 m to 100 m. Such aperture sizes are almost certainly too large to be realized with conventional, full aperture telescopes, and also so large as to probably preclude consideration of adaptive optics in the manner of the CIS-sensor, as the way of getting around atmospheric turbulence limitations. We believe, however, that it is possible to develop the desired SOI imaging capability within these constraints, and shall sketch our approach in the following pages.

The key to the achievement of the desired capability lies in two techniques. They are, first the exploitation of recent developments in speckle imagery, and second the use of a continuously adjustable baseline Michelson stellar interferometer type telescope. With a reasonable length data collection period, appropriate servo systems to control alignment and path length, and sufficient data processing capability this type of system should be able to produce high resolution visible light images of deep space objects. Because of the low apparent angular rate of deep space objects in traveling across the sky, several hours should generally be available for recording the signals necessary to allow the image to be formed. The extent of the required data collection period need not be a fundamental problem.

In this chapter, we shall be concerned with the development of an overview description of this type of deep space satellite speckle imager. We shall point out the areas where we foresee important technical questions

requiring analysis, and will indicate the critical component performance requirements. Finally, we shall indicate the type of performance we may expect from the system.

2.2 Basic Considerations

For space object identification by inspection of imagery, we may take as our basic requirement a resolution of $\delta = 15 \text{ cm}$ ($\approx 6 \text{ inches}$). This is, of course, a somewhat arbitrary choice — but represents what we believe is necessary if we are to be able to do more than simply guess about the objects identity and function based on gross features. If we identify this resolution scale, δ , with the spatial frequency half wavelength at half the apertures cut-off spatial frequency, \mathcal{D}/λ , we find that for an object at range, R , we require

$$[(\frac{1}{2} \mathcal{D}/\lambda)^{-1}] R = 2\delta$$

or

$$\delta = R \lambda / \mathcal{D} \quad . \quad (1)$$

Here λ denotes the operating wavelength, which we may take to be $\lambda = 0.55 \times 10^{-6} \text{ m}$, while \mathcal{D} denotes the maximum separation between points on the collection aperture. For a full aperture system (i. e., a simple circular aperture) \mathcal{D} represents the aperture diameter, while for a Michelson stellar interferometer type telescope, \mathcal{D} denotes the maximum achievable separation between points one in each of the two sub apertures.

For imaging of an object in a synchronous orbit, where $R \approx 3.6 \times 10^7$ m, the required aperture extent is

$$\begin{aligned} \mathcal{D} &= R\lambda/\delta \\ &= 132 \text{ m} \end{aligned} \quad (2)$$

This is so large that it is immediately obvious that we cannot consider a full aperture system.

Even for an object at one-tenth that range (i.e., $R = 3.6 \times 10^6$ m) the required aperture diameter (i.e., $\mathcal{D} = 13.2$ m) is so large that consideration of a full aperture system is at least questionable. Thus, we may conclude that we must, of necessity, contemplate a synthetic aperture type system. We postulate that the realization of this synthetic aperture system will be based on the Michelson stellar interferometer type telescope. In the balance of this work we will take this conclusion for granted. The nominal form of the Michelson stellar interferometer telescope is shown in Figure 1.

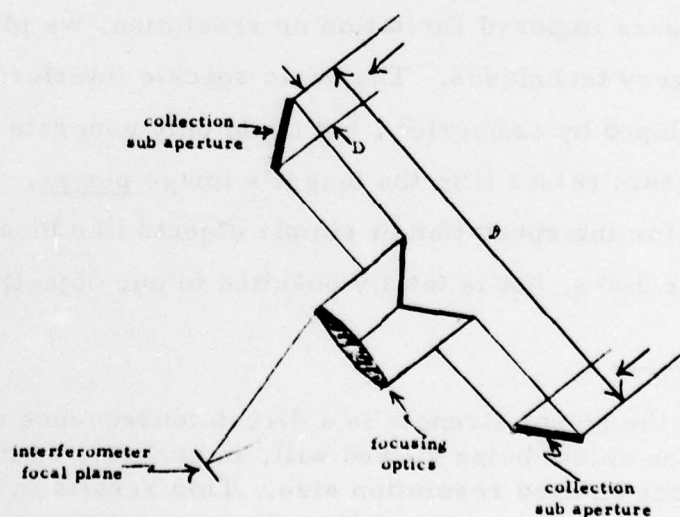


Figure 1. Nominal Form of Michelson Stellar Interferometer.

The sub aperture is D and the baseline size is B .

Atmospheric turbulence will, in general, limit the angular resolution of conventional imaging techniques (whether formed with a full aperture telescope or a Michelson stellar interferometer type telescope) to $\delta \approx 5 \times 10^{-6}$ rad, or larger. This resolution is, of course, incompatible with the desired performance, corresponding to a resolution length $\delta = 180$ m at a synchronous orbit range of $R = 3.6 \times 10^7$ m. The use of adaptive optics to compensate for turbulence effects is precluded first of all by the very weak signal strength to be expected in the self-referenced adaptive optics compensation mode*, but perhaps more significantly, by the fact that available wavefront distortion sensing techniques are all, in essence, shearing interferometer or Hartman sensor methods. These methods are only applicable if there is no significant gap between any two portions of the aperture. But, of course, for the Michelson stellar interferometer type of telescope there are very substantial gaps — so that we have no available wavefront distortion sensing technique around which we can design an adaptive optics compensated imaging system.

In order to avoid this basic limitation, and yet circumvent the atmospheric turbulence imposed limitation on resolution, we plan to make use of speckle imagery techniques. The basic speckle interferometry technique was developed by Labeyrie¹, but could only generate a high resolution correlogram rather than the target's image per se. The correlogram is useful for interpretation of simple objects like binary stars and resolved stellar disks, but is totally unsuited to our objective of space

* The weakness of the signal strength is a direct consequence of the fact that the size of the object being viewed will, in general, be much less than the turbulence limited resolution size. This results in a very low value of target brightness measured in stellar magnitudes per resolution element, and it is this quantity that determines the noise limitation in the performance of self referenced adaptive optics.

object identification. More recently, Knox and Thompson² have extended Labeyrie's technique to allow for true image recovery from speckle data of even very complex objects. The validity of this technique has since been demonstrated in computer simulation by Nisenson, Ehn, and Stacknik³. Thus there is nothing new about the idea of using speckle imagery techniques for SOI. Our particular innovation lies in the concept of applying speckle imagery techniques to data taken with a variable baseline Michelson stellar interferometer type telescope, and in the particular form of this optical configuration.

Because of our plans to use a Michelson stellar interferometer, a very large number of short exposures will have to be formed. Of the order of 10^2 to 10^3 will be required for each baseline setting. This is needed to provide adequate statistical averaging. Moreover, since the interferometer can handle only one limited set of spatial frequencies at a time, a large number of interferometer settings will be required. We shall suggest a design for which about 1000 settings are required for observation of a satellite in a synchronous orbit. Thus between 10^5 and 10^6 total short exposures will have to be generated with each exposure lasting about 10^{-2} sec, this will require between about 20 minutes* and 3 hours for the total image recording process. For a satellite in a lower orbit because a smaller maximum value of the baseline, B , is required to provide the desired resolution, a lesser number of interferometer baseline setting is needed, and so the total image recording time will be smaller. The time should vary about as the square of the satellite altitude or range.

Because we intend to rapidly vary the interferometer baseline it will be necessary to introduce servo controls to handle alignment and equalization of the path length of the two arms of the interferometer. The path length

* This ignores time required to vary the interferometer baseline setting.

equalization servo will, of necessity, be based on white light fringe sensing. If this servo is run with a high enough servo bandwidth, it will not only provide basic alignment control, but will also reduce the turbulence imposed limitation on the allowable spectral bandwidth. This should have a major impact on the required short exposure time.

With this introduction and consideration of basic matters we are now ready to take up the matter of providing a description and definition of the interferometer speckle imaging system. This is treated in the next section.

2.3 System Description

The system consists of four basic components. The first of these is a very flat semicircular concrete surface with a radius $L = 132$ m, which we shall refer to as the "apron." The second component, located at the center of the circle, of which the semicircle is a part, is a $D = 4$ m diameter telescope, which we shall refer to as the "base aperture." The third component of the system is a $d = 1$ m diameter telescope mounted on a mobile base and able to position itself anywhere on the apron. We refer to this as the "mobile aperture." The fourth and last of the basic components is a mobile optical system to which both the base aperture and the mobile aperture relay the radiation received from their field-of-view. In this unit, which we call the "speckle former," the beams from the two apertures are combined to form the desired speckle pattern.

The speckle former unit contains the basic servo capabilities that result in the images formed by the two apertures being properly registered with respect to each other. It also contains the basic white light fringe path length equalization servo. The two aperture units, i. e., the base aperture unit and the mobile aperture unit each have pointing servos to allow them to

track the target being observed and to direct their output beams to the entrance ports of the speckle former unit. These, however, are relatively modest performance servos compared to those in the speckle former unit. It is, in fact, the angular alignment (i. e., the two beam registration) and the path length equalization servos in the speckle former unit that will produce the necessary degree of optical alignment tolerance needed to allow the two arms of the interferometer to work together, in a quasi coherent manner*. Because the mobile aperture unit is continuously moving, the performance of these servos is critical to the ability of the system to function.

The angle tracking alignment achieved in the speckle forming unit is merely good enough to keep two low resolution (turbulence limited) spots reasonably well superimposed on each other. The path length equalization part of the speckle forming units servo control is required to insure that the optical path lengths from the source to the speckle forming unit's focal plane via the base aperture and via the mobile aperture are equal. To accomplish this the speckle forming unit has to be positioned part way between the base aperture and the mobile aperture. (Like the mobile aperture, the speckle forming unit will have to be continuously moving on the apron.) If the target were directly overhead, the speckle forming unit would have to be located exactly half way between the two apertures, but with a target located away from the zenith the speckle forming unit would have to be positioned closer to one aperture than to the other. In all cases the criteria for the speckle forming unit to be in a satisfactory position is that white light interference fringes can be formed in its focal plane. Obviously,

* Actually, because of the nature of speckle imagery, the quasi coherence requirement is considerably less severe than we would have if we required full coherence.

it will not be possible to control the speckle forming units position with sufficient accuracy to insure this. Accordingly, a fine path length adjusting element will be incorporated into the optical train within the speckle forming unit. This path length adjustment element will be servo controlled using, as a basis for generation of a servo error signal, a type of white light fringe visibility sensor. This will not only compensate for geometric path length effects, but will also accommodate the grosser aspects of the turbulence induced path length variations. This will substantially increase the allowed spectral bandwidth — from a nominal value of $\Delta\lambda \approx (r_0/L)\lambda \approx (0.1/132) 5000 \text{ \AA} = 3.8 \text{ \AA}$ based on the turbulence effects over the full interferometer baseline to $\Delta\lambda \approx (r_0/D)\lambda \approx (0.1/4) 5000 \text{ \AA} = 125 \text{ \AA}$, which value is set by the turbulence effects across the larger sub aperture only. The key to this improvement is that the path length servo in the speckle forming unit be fast enough to track the large scale (and therefore, relatively slowly changing) turbulence variations.

To facilitate visualization of the overall system, in Figure 2 we have depicted the several units making up the system, as they might appear on the apron. In the following sections we describe some of the more significant features of each unit. We will then describe the more subtle aspects of the system's principles of operation, and finally will provide some estimates of the expected performance.

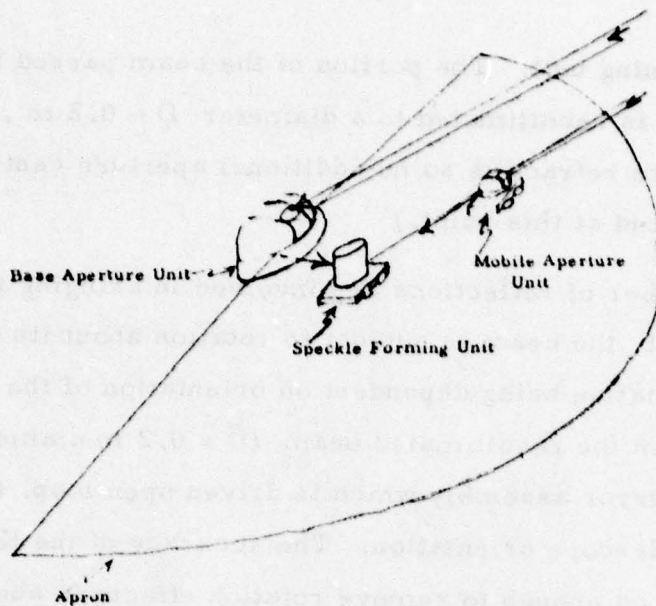


Figure 2. Overview of Synthetic Aperture Speckle Imagery System.

The apron is a very flat concrete surface covering a semicircle of 132 m radius. The mobile aperture unit has an aperture of 1 m diameter while the base aperture unit has an aperture of 4 m diameter. The speckle unit is so positioned that the optical path length from the source to the speckle unit via the two collection apertures are essentially equal.

2.4 Base Aperture Unit

The base aperture unit consists of a $D = 4$ m diameter telescope (in a fixed position dome), with auxiliary optical and servo units. The exact form of the telescope mount (i. e. , altitude inside azimuth, polar axis, etc.) is relatively immaterial. What is important is that the telescope aperture have only a rather small central obscuration (much less than one meter in diameter), and that by some means (nominally a hollow-axis gimbal system) the telescope focus be brought off the mount so its position is stationary, i. e. , independent of the telescope's orientation. The converging beam, just before it reaches the focal plane is beam split by a dichroic filter, splitting off about a 1000 \AA portion around $\lambda = 5500 \text{ \AA}$, for use in forming the speckle image and in generating control signals for

the speckle image forming unit. The portion of the beam passed by the dichroic beam splitter is recollimated to a diameter $\tilde{D} \approx 0.2 \text{ m}$. (The recollimating optics are refractive so no additional aperture central obscuration is introduced at this point.)

Because a number of reflections are involved in bringing the beam off the telescope mount, the beam is subject to rotation about its own axis, the exact amount of rotation being dependent on orientation of the telescope. To remove this rotation the recollimated beam ($\tilde{D} = 0.2 \text{ m}$ diameter) is passed through a K-mirror assembly which is driven open loop, an amount calculated from the telescope orientation. The accuracy of the K-mirror setting need only be good enough to remove rotation effects to about $\pm 1^\circ$. (Fine rotation corrections will be made later on a servo controlled K-mirror device in the speckle forming unit.)

Finally, the recollimated beam is reflected off of a two axis beam steering unit, and transmitted to a beam receiver aperture of the speckle forming unit. To insure accurate positioning of the beam on the receiver aperture of the speckle forming unit, an infrared "pilot beam" is transmitted from that receiver aperture and sensed by a unit that looks through the two axis beam steerer, and also views the direction of the recollimated beam.

The general layout of the base aperture unit is indicated in Figure 3.

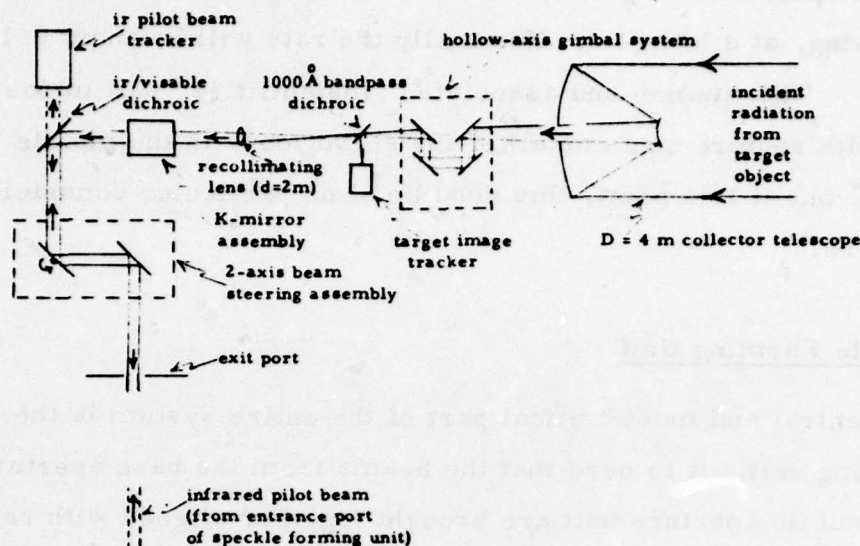


Figure 3. Optical Block Diagram for Base Aperture Unit.

2.5 Mobile Aperture Unit

The mobile aperture unit, considered as an optical train will be essentially the same as the base aperture unit, except for the fact that the telescope aperture diameter will be $d = 1.0 \text{ m}$, and the recollimated beam diameter will be $\tilde{d} = 0.05 \text{ m}$. This beam will also be transmitted to the speckle forming unit, but will enter through its own receiver port. The mobile aperture unit will have the same sort of recollimation optics, dichroic beam splitter, telescope pointing control sensor, K-mirror, and two axis beam steering mirror as the base aperture unit. Of course, they will be matched to a $\tilde{d} = 0.05 \text{ m}$, (rather than a $\tilde{D} = 0.2 \text{ m}$) recollimated beam diameter.

Aside from telescope aperture and recollimated beam diameter differences, the most substantial differences between the base aperture unit and the mobile aperture unit, is the fact that the mobile aperture unit will be mounted on some sort of vehicle and will be able to move about on

the apron. In operation we plan to have the mobile aperture unit continuously moving, at a low rate. Nominally the rate will be about 0.1 to 1.0 m/sec. This motion and associated "instabilities" will impose servo bandwidth requirements on all of the servo loops in the mobile aperture unit, but at this point, this need be of no particular consideration to us here.

2.6 Speckle Forming Unit

The central and most critical part of the entire system is the speckle forming unit. It is here that the beams from the base aperture unit and the mobile aperture unit are brought together aligned with respect to each other in angle and in path length, and then combined on a common focal plane to form the desired image. The speckle forming unit, like the mobile aperture unit, is mounted on wheels and moves on the apron.

Its position is always part way between the base aperture and the mobile aperture, the nominal position being controlled in accordance with the geometric considerations indicated in Figure 4, to equalize the path length via the two apertures. The speckle forming unit utilizes a laser radar unit to measure the distance to the base aperture unit and to the mobile aperture unit, but only to get into approximately the correct position. Fine adjustment of the path length is made on the beam from the mobile aperture unit, after it has entered the port in the speckle forming unit. The adjustments are accomplished with a device of the form shown in Figure 5, which we refer to as the optical path expander.

The signal to control the optical path expander setting is obtained from a quasi white light interferometer unit. The unit combines equal diameter portions of the beams from the base aperture unit and from the mobile aperture unit by means of a beam splitter. The diameter of each

portion will correspond to a diameter of about $\frac{1}{2} r_0$, i.e., about 0.05 m back at the collection apertures. Before being combined at the 50:50 beam splitter/combiner, one path will be phase modulated with a piezoelectrically driven mirror, about $\pm 500 \text{ \AA}$, at a modulation frequency of, say, $3 \times 10^3 \text{ Hz}$. After being combined the composite beam will be reflected off of a diffraction grating and then focused on an intensified linear detector array, with the individual detectors having a spectral resolution of $\Delta\lambda = 1 \text{ \AA}$, and there being a total of 1000 detectors. The optical configuration is indicated in Figure 6.

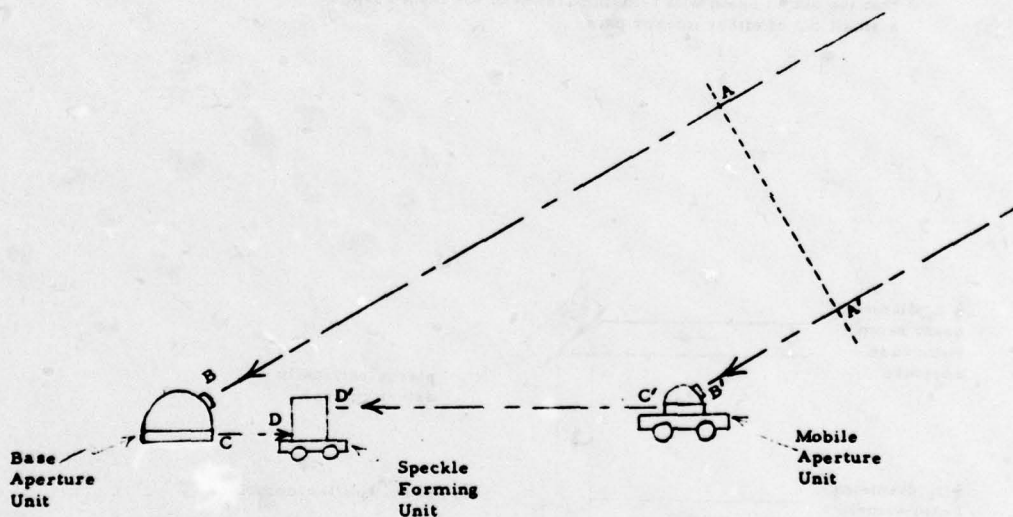


Figure 4. Speckle Forming Unit Positioning Considerations.

A white light fringe condition must be satisfied in order for a useful speckle pattern to be formed. To achieve this the speckle forming unit must be positioned so that $AB + CD \approx A'B' + C'D'$, where the approximation reflects the fact that allowance must be made for optical path lengths within the base aperture unit, the mobile aperture unit, and the speckle forming unit.

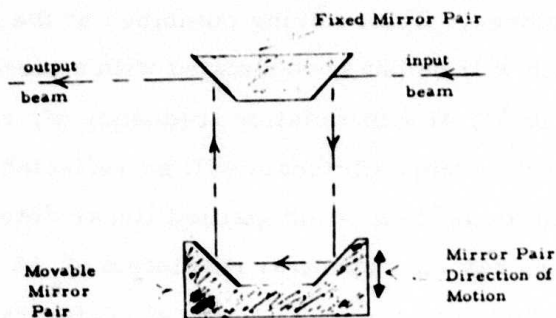


Figure 5. Optical Path Expander.

The optical path length from input to output can be varied, (without effecting any other property at the optical beam) by varying the separation between the fixed mirror pair and the movable mirror pair. It is perhaps worth noting that the output beam will remain parallel to the input despite a small tilt of either mirror pair.

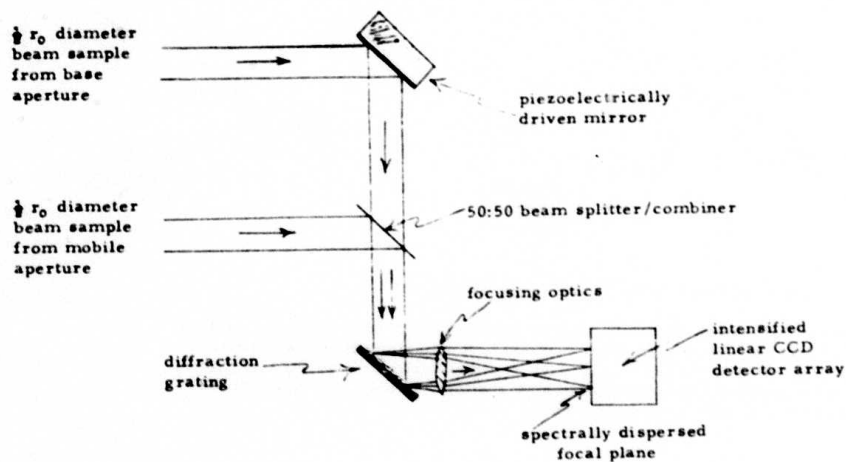


Figure 6. White Light Interferometer Optical Layout.

In operation the optical path expander setting will be slowly moved through a path length variation range of perhaps as much as 1.0 m, though more likely a search over a range of 0.1 m should be sufficient. For the $\Delta\lambda = 1 \text{ \AA}$ spectral resolution at the spectrally dispersed focal plane, when the path expander setting makes the paths nearly equal (in this case to within about $\pm 1.25 \text{ mm}$), the individual detectors will see intensity oscillations at the 3 kHz phase modulation frequency. The exact setting of the path length expander can then be refined by comparing the phase of the modulation signal as seen by each of the detectors. With suitable data processing the path lengths can eventually be equalized to within a fraction of a wavelength, in which case, all of the detectors will see inphase modulation of 3 kHz, and the sum of the detector outputs, i. e., the composite output signal will show strong modulation at this frequency.

The initial alignment of the optical path length expander will be performed with both the mobile aperture unit and the speckle forming unit stationary. Once the white light fringe condition is achieved the two units will be allowed to move. The path length expander device's setting will be controlled by means of a relatively slow dither of the setting, say at 200 Hz over $\pm 200 \text{ \AA}$. It will be observed that the depth of modulation of the 3 kHz variation in the composite signal will oscillate at a 200 Hz rate. The nature of this oscillation will indicate the magnitude and direction of the required correction of the optical path expander's setting, thus providing a basis for closed loop control of the path length equalization. To the extent that the optical path expander setting is away from the middle of its range, this can be used to fine tune the motion of the speckle forming unit as it follows the motion of the mobile aperture unit.

With the path lengths equalized the main portion of the speckle forming unit can now come into play. To form the speckle pattern, the optics "simulates" the desired portion of a $L = 132 \text{ m}$ diameter aperture,

f/50 optical system. The desired portions of the aperture are two circular regions corresponding to $D = 4$ m diameter and $d = 1$ m diameter with a separation corresponding to the current separation, \mathcal{L} , of the base aperture unit and the mobile aperture unit. It is a simulation of these optics in the sense that the actual entrance aperture is only $\mathcal{D} = 1.32$ m, with an effective focal length of $\mathcal{F} = 66$ m. The two beams are first reduced from their initial diameters of $\tilde{D} = 0.2$ m and $\tilde{d} = 0.05$ m to $D' = 0.04$ m and $d' = 0.01$ m. They are then put into two periscope arms, each of which can pivot about a point at the center of their injection apertures. The output of the periscope arms are above a $\mathcal{D} = 1.32$ m diameter mirror, which with its secondary optics, has an effective focal length of $\mathcal{F} = 66$ m. The output of the two periscopes is collected by this mirror optics and brought to a focus. If the two spots are properly oriented and positioned so that they overlap*, they will produce a speckle pattern matching that which would have been formed by the corresponding portions of the aperture of an $L = 132$ m aperture diameter, f/50 telescope!

In order to insure that the two beams are properly registered, just before the two beams reach the focal plane they will pass through a dichroic filter which will pass the narrow band portion (about 200 \AA) to be used in forming the speckle image pattern, but will direct the principal part of the energy (i. e., the rest of the 1000 \AA bandwidth) to an imager/tracker section. Using high speed chopping to block first one and then the other of the two beams, the imager/tracker will be able to sense the positioning error of each of the two spots and generate a beam direction error signal. This

* It should be noted that the individual spot sizes will be of the order of $\lambda/r_0 \approx 0.5 \times 10^{-6}/0.1 = 5 \times 10^{-6}$ rad. So long as the registration error between the two spots is random and small compared to λ/r_0 , it can be considered as equivalent to a small increment in the wavefront tilt portion of the optical effects of turbulence, and will be accommodated in the speckle image data processing.

signal can be generated at a high data rate and used to control a two axis fine adjustment pointing units at the input to each of the periscopes. The data rate should be sufficient to allow a servo bandwidth that can track out any residual, high frequency pointing error due to the motion of the mobile aperture unit or of the speckle forming unit.

In addition, in order to correct for any residual rotation about the beam axis error, the imager/tracker will look for any secondary objects in the field-of-view such as a star which is momentarily near the object, and will determine the K-mirror rotation correction required to make the two beams match. This will be implemented by a fine control K-mirror corrector located just after the port for the beam from the base aperture unit. The data rate for control of this K-mirror will probably be fairly low, but since the required rotation correction should only change rather slowly, this should prove adequate.

In Figure 7 we indicate the optical train associated with the speckle forming unit from the two entrance ports to the two periscopes to the speckle and the tracker/imager focal planes.

With the nature of the basic units thus defined we are now ready to consider the operational procedure and the nominal performance parameters. We take this up in the following sections.

2.7 Operational Procedure

When a target of interest reaches a position in the sky where we wish to start recording its speckle image the mobile aperture unit will be moved to within four meters of the base aperture unit. The speckle forming unit will be positioned near the two aperture units, and so located and operated, that it can receive the two reduced diameter beams sent to it from the base aperture unit and the mobile aperture unit.

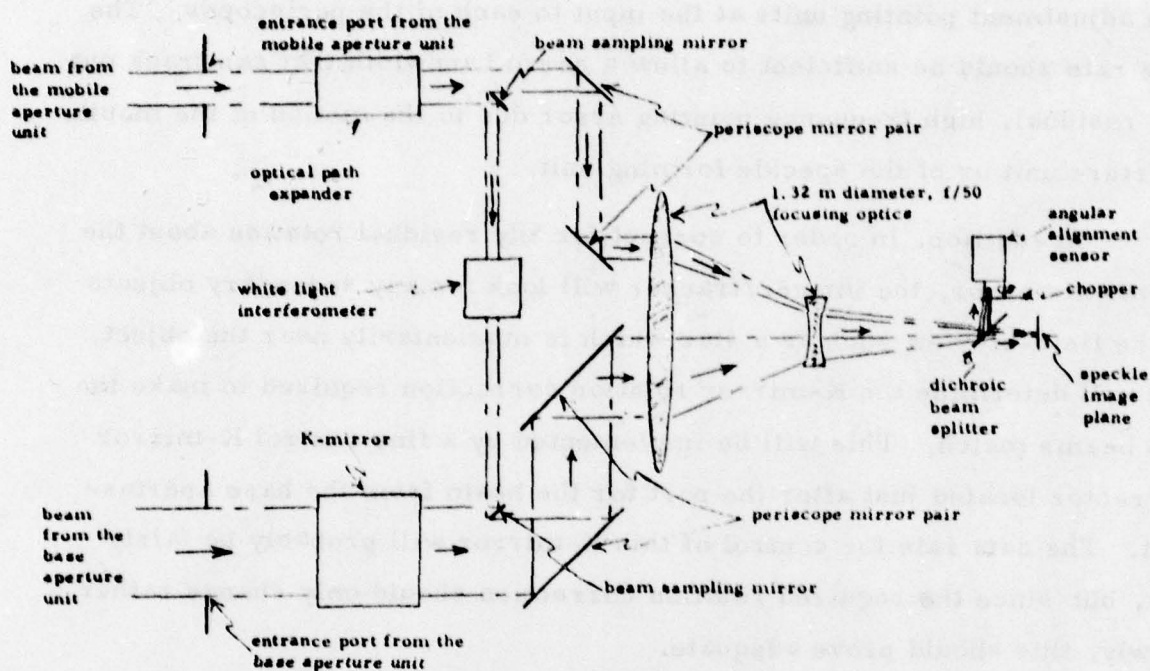


Figure 7. Optical Layout of the Speckle Forming Unit.

At this point, the two telescopes will be pointed toward the target and start to track it. The required tracking precision will be $5 \mu\text{rad}$, $(2-\sigma)$. After passing the collected beam in each aperture unit through a field-stop and a dichroic beam splitter (which stripped out the spectral portion of the beam to be used for tracking), the portion of the beam to be sent to the speckle forming unit will be recollimated and directed to the appropriate entrance port of the speckle forming unit. There the two beams will be combined at a 50:50 beam splitter, after one of the beams has gone through the path length expander. (A selected spectral portion of each of the two beams will have first been split off to be used in forming the speckle image.) The combined beams, "joined" at the 50:50 beam splitter/combiner, will be reflected off a diffraction grating and sent to an array of detectors, each detector corresponding to a narrow spectral band.

The path length expander will be slowly scanned through its control range. Because one of the two beams going into the 50:50 beam splitter/combiner was subject to a 3 kHz phase modulation, when the two path lengths are nearly equal, i. e., the path length expander is near its proper setting, the signal on each detector will be observed to have a significant 3 kHz modulation. At this point, using the small amplitude, 200 Hz modulation of the path length expander, a servo loop is closed to make the path lengths equal. At the same time portions of the two beams going to the speckle imaging plane have been diverted to the imager/tracker sensor where control signals were generated to get the angular alignment of the two received beams adjusted, so that on the speckle image plane the two are registered on each other to within a small fraction of λ/r_0 . At this point, the system will be almost ready to start recording speckle images.

Before the system is fully ready to start the recording of speckle images, the beam rotation will have to be adjusted through the K-mirror assembly in the speckle image unit. This will be done by slowly nodding first one telescope and then the other along the great circle that passes through the zenith, while continuously tracking the target. This will cause the image as seen at the imager/tracker to similarly nod. (The nodding amplitude need only be a few arc seconds.) The K-mirrors will then be adjusted so that both beams produce images that nod back and forth along the same (or parallel) paths. With the K-mirrors thus adjusted, the system will be fully ready to record short exposure speckle images.

The individual short exposures will be allowed 10 msec each. During any one exposure a range of spatial frequencies is recorded corresponding to a 4 m diameter range, i. e., to a range of $|\Delta\vec{x}| = D/\lambda = 4/(\cdot 5 \times 10^{-6}) = 8 \times 10^5$. The mobile aperture unit will be continuously

moving so that a slightly different set of spatial frequencies is recorded in each frame. Because we desire between 10^2 and 10^3 exposures containing each spatial frequency, the speed of the mobile aperture unit will correspond to 4 m displacement in 10^2 to 10^3 , 10 msec exposures, i. e., 4 m/sec to 0.4 m/sec. With this speed the mobile aperture unit will traverse a semicircle about the base aperture unit, and then increment its distance from the base aperture unit by 4 m and repeat its semicircular motion. At the end of each semicircular traverse the distance to the base aperture unit will be incremented, until finally the last traverse will be made at a separation between the mobile aperture unit and the base aperture unit that corresponds to the desired resolution. This will depend principally on the range to the target, the total traverse time, and path length being proportional to the range to the target.

In practice it may prove convenient to move the mobile aperture unit at twice (or three times) the nominal speed and increment the radius of the semicircle by one-half (or one-third) of the nominal 4 m increment. This will reduce the number of short exposures containing any one spatial frequency during a single semicircular traverse, but will cause that spatial frequency to be contained in speckle images recorded on other traverses.

During the system's operation it will, of course, be necessary not only to record each speckle image, but also to record the location of the mobile aperture unit since this will determine the actual spatial frequency content of the image. In addition, it will be necessary to develop the speckle imagery/turbulence transfer function for each spatial frequency. This can be obtained by taking advantage of the periodic presence of a star in the field-of-view near the target object. At 14^{th} magnitude there are an average of 250 stars per square degree. Thus, whenever the target's

angular position moves by one degree relative to the celestial background, approximately 2.87 stars will have passed within $\pm 100 \mu\text{rad}$ of the target object. The speckle forming unit will be designed to split off the image of such a star and form a speckle image on a separate focal plane. In this way speckle calibration data can be obtained for various spatial frequencies*. There will, of course, be sizable gaps in the spatial frequency calibration data because of the uncontrolled nature of the separation between the base aperture unit and the mobile aperture unit at the time when a useful star moves into the field-of-view, but because of the smoothness of the calibration function versus spatial frequency, there should be no problem in interpolating to fill in the missing data.

2.8 Total Exposure Time

As noted initially, the total exposure time and the distance the mobile aperture unit will have to travel is proportional to the square of the targets range. For a target at the maximum range of $3.6 \times 10^7 \text{ m}$, we can estimate the mobile aperture travel distance as

$$s = \frac{1}{2} \pi D^2 / \Delta$$

where $D = 132 \text{ m}$ is the maximum separation between the base aperture unit and the mobile aperture unit, and $\Delta = 4 \text{ m}$ is the radial distance between the semicircular paths traversed by the mobile aperture unit. Thus we get

$$s = \frac{1}{2} \pi (132)^2 / 4 = 6.842 \times 10^3 \text{ m} .$$

* Some method of assuring that the star observed is not actually a binary star, or of allowing for that possibility, will have to be implemented.

With a traverse speed of $v = 0.4$ m/sec (corresponding to 1000 exposures of each spatial frequency) the total exposure time will be

$$T = s/v = 6.842 \times 10^3 / 0.4$$

$$= 1.711 \times 10^4 \text{ sec}$$

$$= 4.75 \text{ hrs} \quad .$$

We must, of course, add to this some time for the change from one semi-circle radius to the next semicircle radius, and some time for initial alignment.

The total time required for high resolution photography of a satellite in a synchronous equatorial orbit (range equals 3.6×10^7 m), is thus seen to be rather small. If the range to the satellite were smaller, say 5×10^6 m (or 1×10^7 m) the required exposure time would drop to an even smaller value from 4.75 hours to only 5.5 minutes (or 22 minutes). If the 100 exposures rather than 1000 exposures per spatial frequency, proves to be acceptable, then the exposure time could be reduced by another factor of ten, to a few minutes or even fractions of minutes.

2.9 Conclusions

Based on the general concept definition provided here and the very preliminary analysis which we have gone through, we conclude that it should be possible to use speckle techniques to form high resolution images of objects in deep space. The components required are reasonably sized, and the technology involved is within the state of the art. There are a number of speckle theory problems which need more detailed examination. Amongst these we list the need for a quantitative understanding of spectral bandwidth and exposure time effects, and a theory of photon shot noise and turbulence sampling noise in speckle imagery. The noise effects are studied at a fundamental level in the next chapter.

2.10 References for Chapter 2

1. A. Labeyrie, "High Resolution Techniques in Optical Astronomy," in Progress in Optics Vol. XV, E. Wolf, Ed., (North Holland, Amsterdam 1976).
2. K. T. Knox and B. J. Thompson, "Recovery of Images from Atmospherically Degraded Short-Exposure Photographs," Ap. J. 193, L45 (1974).
3. P. Nisenson, D. C. Ehn, and R. V. Stacknick, "Astronomical Speckle Imaging," in Proc SPIE 75, 83 (1976). Papers presented at the conference on Imaging Through the Atmosphere, Reston, Virginia, March 22-23, 1976.

Chapter 3

Noise in Speckle Interferometry

and

In Speckle Imagery

3.1 Introduction

Speckle interferometry as originally demonstrated by Labeyrie¹ and speckle imagery as defined by Knox and Thompson² provide us with the capability of obtaining information at near the diffraction limit of a telescope when imaging through turbulence. The key consideration is that for these speckle techniques, while the spatial frequencies near the telescope's diffraction limit are substantially attenuated, nominally by a factor of $(D/r_0)^2$, where D is the telescope's aperture diameter and r_0 is the atmospheric turbulence limited coherence diameter^{3,4}, this level of attenuation is not so great that it can not be compensated in the speckle processing procedure without excessive noise effects, if a reasonably large signal-to-noise ratio is available*. The key question thus reduces to how large a signal-to-noise ratio is available in the speckle process.

Because of the complex nature of the speckle processes the matter of evaluating the signal-to-noise ratio is by no means straightforward. Despite the existence of several studies of noise theory for speckle interferometry^{5,7} there still does not appear to be an exact input to output quantitative theory of noise effects in the results of measurements made using speckle techniques. In this chapter, we shall attempt to develop just such a theory for both speckle interferometry and speckle imagery. We shall develop relationships between the spatial frequency contents of the target

* For ordinary long exposure imagery the spatial frequencies near the diffraction limit are present in the recorded image and at least nominally could be recovered by post detection compensation. However, in this case these spatial frequencies are attenuated by a factor of the order of⁵ $\exp[-3.44 (D/r_0)^{5/3}]$. This is, in general, so great an attenuation factor that no reasonably expected signal-to-noise ratio would be sufficient to prevent noise effects from dominating the post detection compensated image if we attempt to compensate for attenuation factors as large as this.

object, the number of detected photons per short exposure, and the number of short exposures, as our input quantities, and the accuracy with which we can determine the magnitude (and phase) of each spatial frequency component of the target object.

There are two fundamental sources of noise (i.e., of error in the final result) for speckle observations through turbulence. These two noise sources derive from 1) the Poisson statistics of the photon detection events, and from 2) the random nature of the turbulence effects. Both of these noise sources have to be considered in estimating the accuracy of measurements derived from speckle observations.

In the next two sections we shall develop the formalism that we will use in this work to obtain averages over these two noise sources. We shall then briefly review speckle interferometry and speckle imagery and define the quantities directly related to the rms error in the final results of speckle interferometry and speckle imagery. The following sections will be quite mathematical/statistical in nature and will develop values for various "moments" of the recorded shot exposure speckle images. Finally, we shall pull all of these results together to obtain estimates for the rms error to be expected in measurement results extracted from the speckle interferometry process and from the speckle imagery process.

3.2 Averaging Formalism: Turbulence

We shall consider some target object which ideally, i. e., in the absence of turbulence or photon detection shot noise effects would produce an image pattern $I_0(\vec{r})$, where \vec{r} is a two-dimensional vector denoting position in the focal plane of our optical system. For convenience we shall measure focal plane position in terms of the corresponding field-of-view position, so that \vec{r} is actually an angular position vector measured in radians.

We note that $I_0(\vec{r})$ is everywhere nonnegative, i. e.,

$$I_0(\vec{r}) \geq 0 \quad . \quad (1)$$

As a matter of practical convenience we define $I_0(\vec{r})$ to be so normalized that

$$\int d\vec{r} I_0(\vec{r}) = 1 \quad . \quad (2)$$

These two equations allow us, if we wish to do so, to interpret $I_0(\vec{r})$ as a probability density!

Because of atmospheric turbulence effects the ideal image pattern will not be formed. For the moment, to limit our attention to the random effects due to atmospheric turbulence and to suppress from consideration the effects due to the Poisson statistics of the photon detection process, we shall consider the target's brightness to be somehow greatly increased so that the photon detection rate is virtually infinite. The image formed in a single short exposure will, in this case, be random in nature but only because of the random nature of the turbulence effects. (With a virtually infinite photon detection rate the Poisson statistics of the photon detection

process will influence the image negligibly.) The recorded image during such a short exposure, which we shall denote by $I(\vec{r})$, will reflect the random nature of the wavefront distortion at the instant of that short exposure. In exactly the same way that we consider the wavefront distortion to be a random function drawn from a turbulence ensemble, we must similarly consider $I(\vec{r})$ to be a random function also drawn from a turbulence ensemble.

The relationship between the random instantaneous photon noise-free image pattern, $I(\vec{r})$, and the ideal image pattern $I_0(\vec{r})$ is most easily expressed in terms of a random transfer function, $\tau(\vec{\kappa})$, where $\vec{\kappa}$ is a spatial frequency [conjugate to \vec{r} , so that as the dimensions of \vec{r} are radians (field-of-view), the dimensions of $\vec{\kappa}$ are radians (cyclical) per radian (field-of-view).] The random transfer function relates the random wavefront distortion to the random image pattern. In order to make use of this random transfer function, $\tau(\vec{\kappa})$, we need to consider the spatial frequency transforms of the ideal image, $I_0(\vec{r})$, and of the random image, $I(\vec{r})$. We may write these as

$$\tilde{I}_0(\vec{\kappa}) = \int d\vec{r} \exp(-i \vec{\kappa} \cdot \vec{r}) I_0(\vec{r}) \quad , \quad (3)$$

and

$$\tilde{I}(\vec{\kappa}) = \int d\vec{r} \exp(-i \vec{\kappa} \cdot \vec{r}) I(\vec{r}) \quad , \quad (4)$$

respectively. The inverse fourier transform relationships are

$$I_0(\vec{r}) = (2\pi)^{-2} \int d\vec{\kappa} \exp(i \vec{\kappa} \cdot \vec{r}) \tilde{I}_0(\vec{\kappa}) \quad , \quad (5)$$

and

$$I(\vec{r}) = (2\pi)^{-2} \int d\vec{\kappa} \exp(i \vec{\kappa} \cdot \vec{r}) \tilde{I}(\vec{\kappa}) \quad . \quad (6)$$

The random instantaneous transfer function, $\tau(\vec{\kappa})$, characterizing the instantaneous random wavefront distortion relates the random image, $I(\vec{r})$, to the ideal image $I_0(\vec{r})$ by the expression⁵

$$\tilde{I}(\vec{\kappa}) = \tau(\vec{\kappa}) \tilde{I}_0(\vec{\kappa}) \quad , \quad (7)$$

and the associated relationship, based on Eq. 's (3) and (6) in conjunction with Eq. (7), that

$$\begin{aligned} I(\vec{r}) &= (2\pi)^{-2} \int d\vec{\kappa} \exp(i \vec{\kappa} \cdot \vec{r}) \tau(\vec{\kappa}) \int d\vec{r}' \exp(-i \vec{\kappa} \cdot \vec{r}') I_0(\vec{r}') \\ &= (2\pi)^{-2} \iint d\vec{\kappa} d\vec{r}' \exp[i \vec{\kappa} \cdot (\vec{r} - \vec{r}')] \tau(\vec{\kappa}) I_0(\vec{r}') \quad . \quad (8) \end{aligned}$$

For our purposes Eq. (7) rather than Eq. (8) may be taken as the basic relationship.

In accordance with standard procedures the random transfer function is normalized to have a value of unity at zero spatial frequency, i. e.,

$$\tau(0) = 1 \quad , \quad (9)$$

so that the random transfer function can be written in terms of the random pupil function, $P(\vec{\rho})$, as⁸

$$\tau(\vec{\kappa}) = A^{-1} \int d\vec{\rho} P^*(\vec{\rho} + \lambda \vec{\kappa}) P(\vec{\rho}) \quad , \quad (10)$$

where $\vec{\rho}$ is a two-dimensional vector denoting position on the telescope's entrance aperture (measured in units of length), and $P(\vec{\rho})$ represents the random pupil function. The optical wavelength is denoted by λ , so that since $\vec{\kappa}$ has dimensions of radians (cyclical) per radian (field-of-view),

$\lambda \vec{\kappa}$ is a position vector with dimensions comparable to $\vec{\rho}$. The quantity A in Eq. (9) denotes the effective optical power input to the aperture, i. e.,

$$A = \int d\vec{\rho} |P(\vec{\rho})|^2, \quad (11)$$

which in conjunction with Eq. (10) insures the validity of Eq. (9).

For our purposes we may consider the optics, per se, to be aberration free. Thus, if we use the notation $\psi(\vec{\rho})$ to denote the random complex phase shift associated with the turbulence induced random wave-front distortion of some instant, then we can write the pupil function as

$$P(\vec{\rho}) = W(\vec{\rho}) \exp[i\psi(\vec{\rho})]. \quad (12)$$

Here $W(\vec{\rho})$ is a function which serves to define the extent of the telescope's entrance aperture. It is defined by the equation

$$W(\vec{\rho}) = \begin{cases} 1, & \text{if } \vec{\rho} \text{ is inside the aperture} \\ 0, & \text{if } \vec{\rho} \text{ is outside the aperture} \end{cases}. \quad (13)$$

We note here that it is the random nature of $\psi(\vec{\rho})$ that causes the pupil function, $P(\vec{\rho})$, to be a random function. The random nature of $P(\vec{\rho})$ causes the transfer function, $\tau(\vec{\kappa})$, to be a random function. The random nature of $\tau(\vec{\kappa})$, in its turn, causes the photon noise-free instantaneous image pattern, $I(\vec{r})$, and its fourier transform, $\tilde{I}(\vec{\kappa})$, to be random functions. All of these random functions are random in the sense of a selection over the ensemble of turbulence realizations. We shall use the notation $\langle f \rangle_T$ to denote an average of some random function, f , over turbulence, i. e., over the ensemble of all possible realizations of the turbulence pattern and the associated values of f .

We would write, for example, for the mean and mean-square optical transfer function at spatial frequency $\vec{\kappa}$, $\langle \tau(\vec{\kappa}) \rangle_T$, and $\langle |\tau(\vec{\kappa})|^2 \rangle_T$, respectively. Making use of Eq. (10), and of the fact that the ensemble averaging process is linear and therefore commutes with the integration process, we could write

$$\begin{aligned} \langle \tau(\vec{\kappa}) \rangle_T &= \langle A^{-1} \int d\vec{\rho} P^*(\vec{\rho} + \lambda \vec{\kappa}) P(\vec{\rho}) \rangle_T \\ &= A^{-1} \int d\vec{\rho} \langle P^*(\vec{\rho} + \lambda \vec{\kappa}) P(\vec{\rho}) \rangle_T . \end{aligned} \quad (14)$$

Similarly we could write

$$\begin{aligned} \langle |\tau(\vec{\kappa})|^2 \rangle_T &= \langle [A^{-1} \int d\vec{\rho} P^*(\vec{\rho} + \lambda \vec{\kappa}) P(\vec{\rho})]^* \\ &\quad \times [A^{-1} \int d\vec{\rho}' P^*(\vec{\rho}' + \lambda \vec{\kappa}) P(\vec{\rho}')] \rangle_T \\ &= \langle A^{-2} \iint d\vec{\rho} d\vec{\rho}' P(\vec{\rho} + \lambda \vec{\kappa}) P^*(\vec{\rho}) \\ &\quad \times P^*(\vec{\rho}' + \lambda \vec{\kappa}) P(\vec{\rho}') \rangle_T \\ &= A^{-2} \iint d\vec{\rho} d\vec{\rho}' \langle P(\vec{\rho} + \lambda \vec{\kappa}) P^*(\vec{\rho}) P^*(\vec{\rho}' + \lambda \vec{\kappa}) P(\vec{\rho}') \rangle_T . \end{aligned} \quad (15)$$

The farther reduction of expressions like those in the right-hand-side of Eq. 's (14) and (15) is a matter which we shall consider later in discussing the averaging over turbulence. At this point, we may consider our formalism for separating the random turbulence induced effects from the random photon detection effects as established, as well as our formalism for writing the turbulence average. We are now ready to turn to the development of a procedure for handling the random nature of the photon detection process. We take this up in the next section.

3.3 Averaging Formalism: Photon Detection

We note here that the random photon noise-free instantaneous image pattern, $I(\vec{r})$, since it corresponds to a local image density is everywhere nonnegative, i. e.,

$$I(\vec{r}) \geq 0 \quad . \quad (16)$$

Moreover, if we make use of Eq. 's (3), (6), and (7), we can write

$$\begin{aligned} \int d\vec{r} I(\vec{r}) &= (2\pi)^{-2} \iiint d\vec{k} d\vec{r} d\vec{r}' \exp[-i\vec{k} \cdot (\vec{r}' - \vec{r})] \\ &\times \tau(\vec{k}) I_0(\vec{r}') \quad . \end{aligned} \quad (17)$$

This expression can be reduced by making use of the fact that the repeated fourier integral recovers the starting function. With \vec{x} , \vec{y} , and \vec{y}' as n-dimensional vectors we can write this property of the repeated fourier integral as

$$\iint d\vec{x} d\vec{y} \exp[\pm i\vec{x} \cdot (\vec{y} - \vec{y}')] h(\vec{y}') = (2\pi)^n h(\vec{y}) \quad , \quad (18)$$

where $h(\vec{y})$ is any reasonably well behaved function. Choosing the minus part of the plus/minus-sign in Eq. (18), associating \vec{k} in Eq. (17) with \vec{y}' in Eq. (18), \vec{r} in Eq. (17) with \vec{x} in Eq. (18), letting \vec{y} in Eq. (18) be set equal to zero, and equating $h(\vec{y}')$ in Eq. (18) with $\tau(\vec{k}) I_0(\vec{r}')$ in Eq. (17), we can use Eq. (18) to allow us to, in effect, perform the \vec{k} - and \vec{r} -integrations in Eq. (17). Thus we can rewrite Eq. (17) as

$$\begin{aligned} \int d\vec{r} I(\vec{r}) &= (2\pi)^{-2} \int d\vec{r}' \{ (2\pi)^2 \tau(0) I_0(\vec{r}') \} \\ &= \tau(0) \int d\vec{r}' I_0(\vec{r}') \quad . \end{aligned} \quad (19)$$

Making use of Eq. 's (2) and (9) this result can be reduced to the form

$$\int d\vec{r} \, I(\vec{r}) = 1 \quad . \quad (20)$$

This result is very significant since it, in conjunction with Eq. (16), allows us to interpret the photon noise-free instantaneous image pattern, $I(\vec{r})$, as a probability density! $I(\vec{r})$ is, in fact, the probability density governing the position distribution for each detected photon. We shall use it to define the probability of a photon being detected at various positions in the focal plane.

The random aspects of the photon detection process can be usefully separated into two parts. The first part concerns the number of photons detected in forming a single short exposure. Through we expect this number to have the mean value \bar{N} , the actual quantity detected in any one short exposure, N , is a random number. The second part concerns the location on the focal plane where each of the N photon detection events actually occurs. At least nominally we expect these events to be distributed in a way that matches the image pattern/probability density, $I(\vec{r})$. In fact, the distribution on the focal plane will be random and the match to the image pattern, $I(\vec{r})$, will be imperfect. In treating photon detection we shall have to take account of these two things jointly so as to fully account for the random nature of the photon detection process.

In treating the random nature of the photon detection process we shall, in general, be treating some random function $K(\vec{r})$ which defines the distribution of photon detection events on the focal plane for a single short exposure. We can write

$$K(\vec{r}) = \sum_{i=1}^N \delta(\vec{r} - \vec{r}_i) \quad , \quad (21)$$

where $\delta(\vec{r} - \vec{r}_i)$ is the Dirac delta function. Here N is a random number representing the number of photon detection events in the short exposure, and \vec{r}_i is a random position vector denoting the location of the i^{th} photon detection event. The value of N is governed by a Poisson distribution with mean value \bar{N} , i.e.,

$$\text{Prob}(N) = \frac{\bar{N}^N}{N!} \exp(-\bar{N}) \quad , \quad (22)$$

while the distribution of \vec{r}_i is governed by the image pattern/probability density $I(\vec{r}_i)$. It follows that the mean value of some function of N , e.g., $f(N)$, averaged over the photon detection statistics is

$$\langle f(N) \rangle_P = \sum_{N=0}^{\infty} \frac{\bar{N}^N}{N!} \exp(-\bar{N}) f(N) \quad , \quad (23)$$

while the average of some function of \vec{r}_i , e.g., $g(\vec{r}_i)$, averaged over the photon detection statistics is

$$\begin{aligned} \langle g(\vec{r}_i) \rangle_P &= \int d\vec{r}_i I(\vec{r}_i) g(\vec{r}_i) \\ &= \int d\vec{r} I(\vec{r}) g(\vec{r}) \quad . \end{aligned} \quad (24)$$

In both Eq. (23) and Eq. (24) the angle bracket notation subscripted P , i.e., $\langle \rangle_P$, denotes an average over the photon statistics.

It is particularly significant to note that the photon detection process is such that each detection event is independent of each other detection event. Thus, with $i \neq i'$, for some function $G(\vec{r}_i, \vec{r}_{i'})$ we can write

$$\langle G(\vec{r}_i, \vec{r}_{i'}) \rangle = \iint d\vec{r}_i d\vec{r}_{i'} I(\vec{r}_i) I(\vec{r}_{i'}) G(\vec{r}_i, \vec{r}_{i'}) \quad , \quad (25)$$

and if $G(\vec{r}_1, \vec{r}_{1'})$ is factorable, i. e. , we can write

$$G(\vec{r}_1, \vec{r}_{1'}) = g_1(\vec{r}_1) g_2(\vec{r}_{1'}) \quad , \quad (26)$$

then

$$\begin{aligned} \langle G(\vec{r}_1, \vec{r}_{1'}) \rangle &= \iint d\vec{r}_1 d\vec{r}_{1'} I(\vec{r}_1) I(\vec{r}_{1'}) g_1(\vec{r}_1) g_2(\vec{r}_{1'}) \\ &= \left\{ \int d\vec{r}_1 I(\vec{r}_1) g_1(\vec{r}_1) \right\} \left\{ \int d\vec{r}_{1'} I(\vec{r}_{1'}) g_2(\vec{r}_{1'}) \right\} \\ &= \left\{ \int d\vec{r} I(\vec{r}) g_1(\vec{r}) \right\} \left\{ \int d\vec{r} I(\vec{r}) g_2(\vec{r}) \right\} \\ &= \langle g_1(\vec{r}) \rangle_p \langle g_2(\vec{r}) \rangle_p \quad . \end{aligned} \quad (27)$$

In our analysis we shall be interested in the average over photon detection statistics of the produce of two functions of the same randomly chosen short exposure. The functions will be of the form

$$G_1 = \sum_{i=1}^N g_1(\vec{r}_i) \quad , \quad (28a)$$

$$G_2 = \sum_{i=1}^N g_2(\vec{r}_i) \quad , \quad (28b)$$

where N has the same random value in both expressions, and the random vectors $\vec{r}_1, \vec{r}_2, \vec{r}_3, \dots, \vec{r}_N$ are identical in the two expressions. We shall be interested in evaluating the quantity

$$\langle G_1 G_2 \rangle_p = \left\langle \sum_{i=1}^N g_1(\vec{r}_i) \sum_{i'=1}^N g_2(\vec{r}_{i'}) \right\rangle_p$$

$$= \left\langle \sum_{i, i'=1}^N g_1(\vec{r}_i) g_2(\vec{r}_{i'}) \right\rangle_p \quad (29)$$

It is convenient to separate the N^2 - terms in this double sum into $N(N-1)$ - terms for which $i \neq i'$ and the N -terms for which $i = i'$.
Thus we can write

$$\begin{aligned} \langle G_1 G_2 \rangle_p &= \left\langle \sum_{\substack{i, i'=1 \\ i \neq i'}}^N g_1(\vec{r}_i) g_2(\vec{r}_{i'}) \right\rangle_p \\ &+ \left\langle \sum_{i=1}^N g_1(\vec{r}_i) g_2(\vec{r}_i) \right\rangle_p \quad (30) \end{aligned}$$

Making use of Eq. (24) we can see that all N -terms in the second ensemble average in Eq. (30) reduce to the same form so that we can write

$$\begin{aligned} \langle G_1 G_2 \rangle_p &= \left\langle \sum_{\substack{i, i'=1 \\ i \neq i'}}^N g_1(\vec{r}_i) g_2(\vec{r}_{i'}) \right\rangle_p \\ &+ \langle N \rangle_p \int d\vec{r} I(\vec{r}) g_1(\vec{r}) g_2(\vec{r}) \quad (31) \end{aligned}$$

Making use of Eq. (27) we can see that when $i \neq i'$, the photon detection event average over $g_1(\vec{r}_i) g_2(\vec{r}_{i'})$ in Eq. (30) can be separated into two distinct averages. Thus, the $N(N-1)$ -terms in this double sum can be written in such a way that we get in place of Eq. (31),

$$\begin{aligned} \langle G_1 G_2 \rangle_p &= \langle N(N-1) \rangle_p \left\{ \int d\vec{r} I(\vec{r}) g_1(\vec{r}) \right\} \left\{ \int d\vec{r} I(\vec{r}) g_2(\vec{r}) \right\} \\ &+ \langle N \rangle_p \left\{ \int d\vec{r} I(\vec{r}) g_1(\vec{r}) g_2(\vec{r}) \right\} \quad (32) \end{aligned}$$

In developing Eq. 's (31) and (32) we have taken advantage of the fact that the integral over \vec{r} , i.e., $\int d\vec{r} I(\vec{r}) \dots$, is, in effect, an average over the photon detection event statistics in and of itself, and therefore, since it is not a random quantity, need not be retained inside the angle brackets. Only the quantities N and $N(N-1)$, which count the number of terms involved in the sum, remain inside the angle brackets. These quantities can be evaluated making use of Eq. (23). In fact, we find using Eq. (23) that

$$\langle N \rangle_p = \bar{N} \quad , \quad (33a)$$

$$\langle N(N-1) \rangle_p = \bar{N}^2 \quad , \quad (33b)$$

and that in general, the Q^{th} factorial moment of N , i.e., $\langle N(N-1)(N-2) \dots (N-Q+1) \rangle_p$ has a value of

$$\langle N(N-1)(N-2) \dots (N-Q+1) \rangle_p = \bar{N}^Q \quad . \quad (34)$$

Making use of these techniques suitably extended to allow for the evaluation of the mean value of the produce of not just two functions of the form of G_1 and G_2 , but of the produce of up to four such functions, we shall be able to develop the photon detection statistics for all of the quantities of interest to us in speckle interferometry and speckle imagery. We carry out the basic evaluations in Section 5. Before turning to that, however, we shall first briefly comment on the formalism for the joint photon-detection-event and wavefront-distortion statistics. We take this up in the next section.

3.4 Averaging Formalism: Photon Detection and Wavefront Distortion

In practice we shall be interested in averages taken over the statistical nature of both the wavefront distortion process and the photon detection process. We shall use the notation of unsubscripted angle brackets, vis., $\langle \rangle$, to denote such a joint average. For evaluation we shall understand that we may replace this average notation with the notation $\langle \langle \rangle_p \rangle_t$, with the understanding that the photon statistics average is always taken within the turbulence (i.e., wavefront distortion) average. This is because the photon statistics average may be expected to be expressed in terms of $I(\vec{r})$, the image pattern/probability density. However, this image pattern is random in the sense of its dependence on turbulence and so the photon detection average taken over $I(\vec{r})$, must then be further averaged to account for the random variability of $I(\vec{r})$ associated with turbulence effects. Hence the requirement that the photon detection average, $\langle \rangle_p$, be enclosed within the angle brackets, $\langle \rangle_t$, denoting the average over turbulence effects.

With this matter settled, we are now ready to turn our attention to evaluating some of the photon detection statistical averages that we will need in evaluating the speckle statistics. We take this up in the next section.

3.5 Spatial Frequency Spectral Moments: Photon Detection Averaging

Speckle interferometry and speckle imagery are both based on manipulation of the spatial frequency transform of the short exposure image. It will therefore prove convenient in our subsequent work if we develop here a set of expressions for the photon detection event statistical averages of various moments of the random amplitudes associated with the fourier transform of a random short exposure image. We develop these results in the following.

The basic random short exposure image pattern is represented by $R(\vec{r})$, which was defined by Eq. (21). In that equation N , as we recall, denotes the random number of photon detection events making up the image, and \vec{r}_i denotes the location of the i^{th} photon detection event. The spatial distribution of \vec{r}_i is governed by the probability density $I(\vec{r}_i)$, which so long as we are considering only the photon detection statistics may be considered to be a well defined quantity. [It is only when we turn to consideration of averages over turbulence that we have to take account of the fact that $I(\vec{r})$ is a random function. In the work of this section we may ignore that fact.] The fourier transform of the random pattern at spatial frequency $\vec{\kappa}_j$ may be written as,

$$R(\vec{\kappa}_j) = \int d\vec{r} \exp(-i \vec{\kappa}_j \cdot \vec{r}) R(\vec{r}) \quad . \quad (35)$$

When we substitute Eq. (21) into Eq. (35), interchange the order of integration and summation, and then use the well known properties of the Dirac delta function to allow us to carry out the \vec{r} -integration, we obtain the result that

$$R(\vec{\kappa}_j) = \sum_{i=1}^N \exp(-i \vec{\kappa}_j \cdot \vec{r}_i) \quad . \quad (36)$$

We shall be interested in the average over photon detection statistics of $R(\vec{\kappa}_j)$ and of the produce of such quantities for different values of $\vec{\kappa}_j$. Because of the fact that

$$R^*(\vec{\kappa}_j) = R(-\vec{\kappa}_j) \quad , \quad (37)$$

we can restrict our attention to the following four averages; namely

$$M_1(\vec{\kappa}_1) = \langle R(\vec{\kappa}_1) \rangle, \quad (38a)$$

$$M_2(\vec{\kappa}_1, \vec{\kappa}_2) = \langle R(\vec{\kappa}_1) R(\vec{\kappa}_2) R(\vec{\kappa}_3) \rangle, \quad (38b)$$

$$M_3(\vec{\kappa}_1, \vec{\kappa}_2, \vec{\kappa}_3) = \langle R(\vec{\kappa}_1) R(\vec{\kappa}_2) R(\vec{\kappa}_3) \rangle, \quad (38c)$$

$$M_4(\vec{\kappa}_1, \vec{\kappa}_2, \vec{\kappa}_3, \vec{\kappa}_4) = \langle R(\vec{\kappa}_1) R(\vec{\kappa}_2) R(\vec{\kappa}_3) R(\vec{\kappa}_4) \rangle. \quad (38d)$$

Starting with the evaluation of M_1 , substituting Eq. (36) into Eq. (38a) we get

$$M_1(\vec{\kappa}_1) = \left\langle \sum_{i=1}^N \exp(-i \vec{\kappa}_1 \cdot \vec{r}_i) \right\rangle. \quad (39)$$

Making use of Eq. (24) and the formalism developed in Section 3, we can rewrite this as

$$\begin{aligned} M_1(\vec{\kappa}_1) &= \langle N \rangle \int d\vec{r} \exp(-i \vec{\kappa}_1 \cdot \vec{r}) I(\vec{r}) \\ &= \bar{N} \tilde{I}(\vec{\kappa}_1) \quad , \end{aligned} \quad (40)$$

where

$$\tilde{I}(\vec{\kappa}) = \int d\vec{r} \exp(-i \vec{\kappa} \cdot \vec{r}) I(\vec{r}) \quad . \quad (41)$$

We note that just as $I(\vec{r})$ is a randomly selected function, held constant within the photon detection statistics, similarly $\tilde{I}(\vec{\kappa})$ is also randomly selected function held constant within the photon detection statistics. [Both $I(\vec{r})$ and $\tilde{I}(\vec{\kappa})$ are randomly selected from the turbulence ensemble.] Just as $I(\vec{r})$ corresponds to a probability density, $\tilde{I}(\vec{\kappa})$ represents the associated generating function.

The evaluation of M_2 follows almost directly from Eq. (32) and the immediately preceding type of manipulations. Starting with Eq. (38b) and substituting Eq. (36) twice, we can write

$$\begin{aligned} M_2(\vec{\kappa}_1, \vec{\kappa}_2) &= \left\langle \sum_{i=1}^N \exp(-i \vec{\kappa}_1 \cdot \vec{r}_i) \sum_{i'=1}^N \exp(-i \vec{\kappa}_2 \cdot \vec{r}_{i'}) \right\rangle, \\ &= \left\langle \sum_{i, i'=1}^N \exp(-i \vec{\kappa}_1 \cdot \vec{r}_i) \exp(-i \vec{\kappa}_2 \cdot \vec{r}_{i'}) \right\rangle, \quad (42) \end{aligned}$$

Following the procedure demonstrated in developing Eq. (32) from Eq. (29), we start by separating the double sum in Eq. (42) into the $N(N-1)$ - terms for which $i \neq i'$ and the N -terms for which $i = i'$. Thus we can write

$$M_2(\vec{\kappa}_1, \vec{\kappa}_2) = \left\langle \sum_{\substack{i, i'=1 \\ i \neq i'}}^N \exp(-i \vec{\kappa}_1 \cdot \vec{r}_i) \exp(-i \vec{\kappa}_2 \cdot \vec{r}_{i'}) \right\rangle,$$

$$+ \left\langle \sum_{i=1}^N \exp[-i(\vec{\kappa}_1 + \vec{\kappa}_2) \cdot \vec{r}_i] \right\rangle, \quad (43)$$

Proceeding just as in the development of Eq. (32) we can replace each of these exponentials by their average over the probability density $I(\vec{r}_i)$ or $I(\vec{r}_{i'})$, and take the average value outside of the angle brackets. The two sums, each with unity as the summand, reduce to $N(N-1)$ and N . Thus, Eq. (43) can be reduced to the form

$$\begin{aligned} M_2(\vec{\kappa}_1, \vec{\kappa}_2) &= \langle N(N-1) \rangle_p \left\{ \int d\vec{r}_i \exp(-i\vec{\kappa}_1 \cdot \vec{r}_i) I(\vec{r}_i) \right\} \\ &\times \left\{ \int d\vec{r}_{i'} \exp(-i\vec{\kappa}_2 \cdot \vec{r}_{i'}) I(\vec{r}_{i'}) \right\} \\ &+ \langle N \rangle_p \left\{ \int d\vec{r}_i \exp[-i(\vec{\kappa}_1 + \vec{\kappa}_2) \cdot \vec{r}_i] I(\vec{r}_i) \right\}. \quad (44) \end{aligned}$$

Making use of Eq.'s (34) and (41) we can reduce this to

$$M_2(\vec{\kappa}_1, \vec{\kappa}_2) = \bar{N}^2 \tilde{I}(\vec{\kappa}_1) \tilde{I}(\vec{\kappa}_2) + \bar{N} \tilde{I}(\vec{\kappa}_1 + \vec{\kappa}_2). \quad (45)$$

This same procedure can now be applied for the evaluation of the higher moments, M_3 and M_4 .

In evaluating M_3 we will encounter a triple sum on i , i' , and i'' and will have to consider a more complex pattern of subdivision of the sum. If we substitute Eq. (36) into Eq. (38c) we get

$$\begin{aligned} M_3(\vec{\kappa}_1, \vec{\kappa}_2, \vec{\kappa}_3) &= \left\langle \sum_{i=1}^N \exp(-i\vec{\kappa}_1 \cdot \vec{r}_i) \sum_{i'=1}^N \exp(-i\vec{\kappa}_2 \cdot \vec{r}_{i'}) \right. \\ &\times \left. \sum_{i''=1}^N \exp(-i\vec{\kappa}_3 \cdot \vec{r}_{i''}) \right\rangle_p, \quad (46) \end{aligned}$$

which when we form a triple sum from the product of three sums, takes the form

$$M_3(\vec{\kappa}_1, \vec{\kappa}_2, \vec{\kappa}_3) = \left\langle \sum_{1,1',1''=1}^N \exp(-i \vec{\kappa}_1 \cdot \vec{r}_1) \exp(-i \vec{\kappa}_2 \cdot \vec{r}_{1'}) \right. \\ \left. \times \exp(-i \vec{\kappa}_3 \cdot \vec{r}_{1''}) \right\rangle, \quad (47)$$

In this case we separate the triple sum, consisting of N^3 -terms, into a sum on the $N(N-1)(N-2)$ -terms [equal to $(N^3 - 3N^2 + 2N)$ -terms] for which $\{i \neq i' \neq i''\}$, three separate double sums of $N(N-1)$ -terms [equal to a total of $(3N^2 - 3N)$ -terms] for which $\{i = i' \neq i''\}$, or $\{i = i'' \neq i'\}$, or $\{i' = i'' \neq i\}$, and the single sum of N -terms for which $\{i = i' = i''\}$. Thus, we can write

$$M_3(\vec{\kappa}_1, \vec{\kappa}_2, \vec{\kappa}_3) = \left\langle \sum_{\substack{1,1',1''=1 \\ i \neq i' \neq i''}}^N \exp(-i \vec{\kappa}_1 \cdot \vec{r}_1) \exp(-i \vec{\kappa}_2 \cdot \vec{r}_{1'}) \exp(-i \vec{\kappa}_3 \cdot \vec{r}_{1''}) \right\rangle, \\ + \left\langle \sum_{\substack{1,1''=1 \\ i \neq 1''}}^N \exp[-i(\vec{\kappa}_1 + \vec{\kappa}_2) \cdot \vec{r}_1] \exp(-i \vec{\kappa}_3 \cdot \vec{r}_{1''}) \right\rangle, \\ + \left\langle \sum_{\substack{1,1'=1 \\ i \neq 1'}}^N \exp[-i(\vec{\kappa}_1 + \vec{\kappa}_3) \cdot \vec{r}_1] \exp(-i \vec{\kappa}_2 \cdot \vec{r}_{1'}) \right\rangle, \\ + \left\langle \sum_{\substack{1,1'=1 \\ i \neq 1'}}^N \exp[-i(\vec{\kappa}_2 + \vec{\kappa}_3) \cdot \vec{r}_{1'}] \exp(-i \vec{\kappa}_1 \cdot \vec{r}_1) \right\rangle, \\ + \left\langle \sum_{i=1}^N \exp[-i(\vec{\kappa}_1 + \vec{\kappa}_2 + \vec{\kappa}_3) \cdot \vec{r}_1] \right\rangle, \quad (48)$$

Averaging over the portion of the photon detection statistics which concerns the location at which each of the N-photons is detected, which is governed by the probability density $I(\vec{r})$, and using the fact that the random variables \vec{r}_1 , $\vec{r}_{1'}$, and $\vec{r}_{1''}$ as they appear in each angle bracket term in Eq. (48) are distributed independently of the others, we can write in place of Eq. (48) that

$$\begin{aligned}
M_3(\vec{\kappa}_1, \vec{\kappa}_2, \vec{\kappa}_3) = & \langle N(N-1)(N-2) \rangle_p \left\{ \int d\vec{r}_1 \exp(-i \vec{\kappa}_1 \cdot \vec{r}_1) I(\vec{r}_1) \right\} \\
& \times \left\{ \int d\vec{r}_{1'} \exp(-i \vec{\kappa}_2 \cdot \vec{r}_{1'}) I(\vec{r}_{1'}) \right\} \left\{ \int d\vec{r}_{1''} \exp(-i \vec{\kappa}_3 \cdot \vec{r}_{1''}) I(\vec{r}_{1''}) \right\} \\
& + \langle N(N-1) \rangle_p \left\{ \int d\vec{r}_1 \exp[-i(\vec{\kappa}_1 + \vec{\kappa}_2) \cdot \vec{r}_1] I(\vec{r}_1) \right\} \\
& \times \left\{ \int d\vec{r}_{1''} \exp(-i \vec{\kappa}_3 \cdot \vec{r}_{1''}) I(\vec{r}_{1''}) \right\} \\
& + \langle N(N-1) \rangle_p \left\{ \int d\vec{r}_1 \exp[-i(\vec{\kappa}_1 + \vec{\kappa}_3) \cdot \vec{r}_1] I(\vec{r}_1) \right\} \\
& \times \left\{ \int d\vec{r}_{1'} \exp(-i \vec{\kappa}_2 \cdot \vec{r}_{1'}) I(\vec{r}_{1'}) \right\} \\
& + \langle N(N-1) \rangle_p \left\{ \int d\vec{r}_{1'} \exp[-i(\vec{\kappa}_2 + \vec{\kappa}_3) \cdot \vec{r}_{1'}] I(\vec{r}_{1'}) \right\} \\
& \times \left\{ \int d\vec{r}_1 \exp(-i \vec{\kappa}_1 \cdot \vec{r}_1) I(\vec{r}_1) \right\} \\
& + \langle N \rangle_p \left\{ \int d\vec{r}_1 \exp[-i(\vec{\kappa}_1 + \vec{\kappa}_2 + \vec{\kappa}_3) \cdot \vec{r}_1] I(\vec{r}_1) \right\} \quad . \quad (49)
\end{aligned}$$

Now, if we make use of Eq. 's (34) and (41) we can reduce this to the much more compact result that

$$M_3(\vec{\kappa}_1, \vec{\kappa}_2, \vec{\kappa}_3) = \bar{N}^3 \tilde{I}(\vec{\kappa}_1) \tilde{I}(\vec{\kappa}_2) \tilde{I}(\vec{\kappa}_3)$$

$$\begin{aligned}
& + \bar{N}^2 \tilde{I}(\vec{\kappa}_1 + \vec{\kappa}_2) \tilde{I}(\vec{\kappa}_3) + \bar{N}^2 \tilde{I}(\vec{\kappa}_1 + \vec{\kappa}_3) \tilde{I}(\vec{\kappa}_2) \\
& + \bar{N}^2 \tilde{I}(\vec{\kappa}_2 + \vec{\kappa}_3) \tilde{I}(\vec{\kappa}_1) + \bar{N} \tilde{I}(\vec{\kappa}_1 + \vec{\kappa}_2 + \vec{\kappa}_3) \quad . \quad (50)
\end{aligned}$$

This same sort of procedure now has to be carried out to evaluate the fourth moment, M_4 .

In evaluating M_4 we initially form a product of four sums which we rewrite as a quadruple sum of N^4 -terms. Thus, we have

$$\begin{aligned}
M_4(\vec{\kappa}_1, \vec{\kappa}_2, \vec{\kappa}_3, \vec{\kappa}_4) &= \left\langle \sum_{i=1}^N \exp(-i \vec{\kappa}_1 \cdot \vec{r}_i) \sum_{i'=1}^N \exp(-i \vec{\kappa}_2 \cdot \vec{r}_{i'}) \right. \\
&\times \sum_{i''=1}^N \exp(-i \vec{\kappa}_3 \cdot \vec{r}_{i''}) \sum_{i'''=1}^N \exp(-i \vec{\kappa}_4 \cdot \vec{r}_{i'''}) \rangle_p \\
&= \left\langle \sum_{i, i', i'', i'''=1}^N \exp(-i \vec{\kappa}_1 \cdot \vec{r}_i) \exp(-i \vec{\kappa}_2 \cdot \vec{r}_{i'}) \right. \\
&\times \exp(-i \vec{\kappa}_3 \cdot \vec{r}_{i''}) \exp(-i \vec{\kappa}_4 \cdot \vec{r}_{i'''}) \rangle_p \quad . \quad (51)
\end{aligned}$$

This sum of N^4 -terms can be separated into the following subsidiary sums:

1) a sum of $N(N-1)(N-2)(N-3)$ -terms for which $\{i \neq i' \neq i'' \neq i'''\}$, 2) six sums of $N(N-1)(N-2)$ -terms for which $\{i = i' \neq i'' \neq i'''\}$, or $\{i = i'' \neq i' \neq i'''\}$, or $\{i = i''' \neq i' \neq i''\}$, or $\{i' = i'' \neq i \neq i'''\}$, or $\{i' = i''' \neq i \neq i''\}$, or $\{i'' = i''' \neq i \neq i'\}$, 3) three sums of $N(N-1)$ -terms for which $\{i = i' \neq i'' = i'''\}$, or $\{i = i'' \neq i' = i'''\}$, or $\{i = i''' \neq i' = i''\}$, 4) four sums of $N(N-1)$ -terms for which $\{i = i' = i'' \neq i'''\}$, or $\{i = i' = i''' \neq i''\}$, or $\{i = i'' = i''' \neq i'\}$, or $\{i' = i'' = i''' \neq i\}$, and 5) one sum of N -terms for which $\{i = i' = i'' = i'''\}$.

Following exactly the same procedures as we used in going from Eq. (47)

to Eq. (50) this separation of the terms in the sum in Eq. (51) and the subsequent reduction will yield the result that

$$\begin{aligned}
M_4(\vec{\kappa}_1, \vec{\kappa}_2, \vec{\kappa}_3, \vec{\kappa}_4) = & \bar{N}^4 \tilde{I}(\vec{\kappa}_1) \tilde{I}(\vec{\kappa}_2) \tilde{I}(\vec{\kappa}_3) \tilde{I}(\vec{\kappa}_4) \\
& + \bar{N}^3 \tilde{I}(\vec{\kappa}_1 + \vec{\kappa}_2) \tilde{I}(\vec{\kappa}_3) \tilde{I}(\vec{\kappa}_4) + \bar{N}^3 \tilde{I}(\vec{\kappa}_1 + \vec{\kappa}_3) \tilde{I}(\vec{\kappa}_2) \tilde{I}(\vec{\kappa}_4) \\
& + \bar{N}^3 \tilde{I}(\vec{\kappa}_1 + \vec{\kappa}_4) \tilde{I}(\vec{\kappa}_2) \tilde{I}(\vec{\kappa}_3) + \bar{N}^3 \tilde{I}(\vec{\kappa}_2 + \vec{\kappa}_3) \tilde{I}(\vec{\kappa}_1) \tilde{I}(\vec{\kappa}_4) \\
& + \bar{N}^3 \tilde{I}(\vec{\kappa}_2 + \vec{\kappa}_4) \tilde{I}(\vec{\kappa}_1) \tilde{I}(\vec{\kappa}_3) + \bar{N}^3 \tilde{I}(\vec{\kappa}_3 + \vec{\kappa}_4) \tilde{I}(\vec{\kappa}_1) \tilde{I}(\vec{\kappa}_2) \\
& + \bar{N}^2 \tilde{I}(\vec{\kappa}_1 + \vec{\kappa}_2) \tilde{I}(\vec{\kappa}_3 + \vec{\kappa}_4) + \bar{N}^2 \tilde{I}(\vec{\kappa}_1 + \vec{\kappa}_3) \tilde{I}(\vec{\kappa}_2 + \vec{\kappa}_4) \\
& + \bar{N}^2 \tilde{I}(\vec{\kappa}_1 + \vec{\kappa}_4) \tilde{I}(\vec{\kappa}_2 + \vec{\kappa}_3) + \bar{N}^2 \tilde{I}(\vec{\kappa}_1 + \vec{\kappa}_2 + \vec{\kappa}_3) \tilde{I}(\vec{\kappa}_4) \\
& + \bar{N}^2 \tilde{I}(\vec{\kappa}_1 + \vec{\kappa}_2 + \vec{\kappa}_4) \tilde{I}(\vec{\kappa}_3) + \bar{N}^2 \tilde{I}(\vec{\kappa}_1 + \vec{\kappa}_3 + \vec{\kappa}_4) \tilde{I}(\vec{\kappa}_2) \\
& + \bar{N}^2 \tilde{I}(\vec{\kappa}_2 + \vec{\kappa}_3 + \vec{\kappa}_4) \tilde{I}(\vec{\kappa}_1) + \bar{N} \tilde{I}(\vec{\kappa}_1 + \vec{\kappa}_2 + \vec{\kappa}_3 + \vec{\kappa}_4) \quad . \quad (52)
\end{aligned}$$

With these results for the first four spectral moments in hand, i. e., M_1 , M_2 , M_3 , and M_4 , as given by Eq. 's (40), (45), (50), and (52) we are now ready to consider the quantities calculated in speckle interferometry and speckle imagery, as averaged over the photon detection statistics. This is treated in the next section.

3.6 Unbiased Speckle Measurement Quantities

In speckle interferometry and speckle imagery the basic measurement is the fourier transform at spatial frequency $\vec{\kappa}$, of the random image pattern recorded during a single short exposure. This corresponds to the quantity $R(\vec{\kappa})$ defined in Eq. (35). Data reduction is based on calculating the mean value of a quantity like $R^*(\vec{\kappa}) R(\vec{\kappa})$ for speckle interferometry and of a quantity like $R^*(\vec{\kappa}') R(\vec{\kappa})$ for speckle imagery. The averaging is over a series of short exposures and thus is, in effect, over both photon detection statistics and over turbulence statistics. Since the expression $R^*(\vec{\kappa}') R(\vec{\kappa})$ for speckle imagery obviously subsumes the expression $R^*(\vec{\kappa}) R(\vec{\kappa})$ for speckle interferometry we shall treat only the former quantity.

The average over many short exposures for this quantity, i. e., $\langle R^*(\vec{\kappa}') R(\vec{\kappa}) \rangle$, which represents an average over both the turbulence dependence and the photon detection effects, can be rewritten using the formalism of Section 4, as

$$\langle R^*(\vec{\kappa}') R(\vec{\kappa}) \rangle = \langle \langle R^*(\vec{\kappa}') R(\vec{\kappa}) \rangle_p \rangle_T. \quad (53)$$

Making use of Eq. 's (37), (38b), and (45) we can rewrite this as

$$\langle R^*(\vec{\kappa}') R(\vec{\kappa}) \rangle = \langle \bar{N}^2 \tilde{I}(-\vec{\kappa}') \tilde{I}(\vec{\kappa}) + \bar{N} \tilde{I}(\vec{\kappa} - \vec{\kappa}') \rangle_T. \quad (54)$$

Now making use of Eq. (7) and removing from inside the angle brackets all the terms which do not depend in a statistical way on the wavefront distortion, we can rewrite Eq. (54) as

$$\begin{aligned} \langle R^*(\vec{\kappa}') R(\vec{\kappa}) \rangle &= \bar{N}^2 \tilde{I}_0(-\vec{\kappa}') \tilde{I}_0(\vec{\kappa}) \langle \tau(-\vec{\kappa}') \tau(\vec{\kappa}) \rangle_T \\ &+ \bar{N} \tilde{I}_0(\vec{\kappa} - \vec{\kappa}') \langle \tau(\vec{\kappa} - \vec{\kappa}') \rangle_T. \end{aligned} \quad (55)$$

We note from Eq. 's (4) and (10) that

$$\tilde{I}_0(-\vec{\kappa}') = \tilde{I}_0^*(\vec{\kappa}) \quad , \quad (56)$$

and that

$$\tau(-\vec{\kappa}') = \tau^*(\vec{\kappa}') \quad , \quad (57)$$

so that Eq. (55) can be rewritten as

$$\begin{aligned} \langle R^*(\vec{\kappa}') R(\vec{\kappa}) \rangle &= \bar{N}^2 \tilde{I}_0^*(\vec{\kappa}') \tilde{I}_0(\vec{\kappa}) \langle \tau^*(\vec{\kappa}') \tau(\vec{\kappa}) \rangle_T \\ &+ \bar{N} \tilde{I}_0(\vec{\kappa} - \vec{\kappa}') \langle \tau(\vec{\kappa} - \vec{\kappa}') \rangle_T \quad . \end{aligned} \quad (58)$$

This result is, in a sense, potentially embarrassing in as much as it indicates that $R^*(\vec{\kappa}') R(\vec{\kappa})$ is a "biased" quantity. We note that $\tilde{I}_0(\vec{\kappa})$ represents the spatial frequency spectral amplitude, at spatial frequency $\vec{\kappa}$, of the object whose pattern, $I_0(\vec{r})$, we are trying to determine. We are entitled to expect that if the object has no spectral amplitude at spatial frequency $\vec{\kappa}$ or $\vec{\kappa}'$ then the average we are evaluating, nominally $\langle R^*(\vec{\kappa}') R(\vec{\kappa}) \rangle$, should have zero value. However, we can see from consideration of Eq. (58) that because of shot noise effects, this average does not vanish when $\tilde{I}_0(\vec{\kappa}')$ or $\tilde{I}_0(\vec{\kappa})$ is zero. There is a residual bias term of the order of $\bar{N} \tilde{I}_0(\vec{\kappa} - \vec{\kappa}') \langle \tau(\vec{\kappa} - \vec{\kappa}') \rangle_T$. Even with large values of \bar{N} , because of the disparity between $\langle \tau(\vec{\kappa} - \vec{\kappa}') \rangle_T$ and $\langle \tau^*(\vec{\kappa}') \tau(\vec{\kappa}) \rangle_T$ when $\vec{\kappa}$ and $\vec{\kappa}'$ are nearly equal and $\vec{\kappa}$ is large (i.e., near the telescope diffraction limit cutoff), this bias term can be substantial compared to the "principle" term in Eq. (58).

In order to avoid this bias term the speckle processor should evaluate the average over a series of short exposures of

$$S(\vec{\kappa}, \vec{\kappa}') = R^*(\vec{\kappa}') R(\vec{\kappa}) - R(\vec{\kappa} - \vec{\kappa}') \quad . \quad (59)$$

It is easy to show that the average of this quantity leads to an unbiased result of the basic form we expect. We can write, using the formalism of Section 4, that

$$\langle S(\vec{\kappa}, \vec{\kappa}') \rangle = \langle \langle S(\vec{\kappa}, \vec{\kappa}') \rangle_p \rangle_T \quad . \quad (60)$$

Substituting Eq. (59) into Eq. (60) we get

$$\langle S(\vec{\kappa}, \vec{\kappa}') \rangle = \langle \langle R^*(\vec{\kappa}') R(\vec{\kappa}) \rangle_p \rangle_T - \langle \langle R(\vec{\kappa} - \vec{\kappa}') \rangle_p \rangle_T \quad . \quad (61)$$

Making use of Eq. (58) as well as of Eq. 's (38a) and (40) allows us to rewrite Eq. (61) as

$$\begin{aligned} \langle S(\vec{\kappa}, \vec{\kappa}') \rangle &= \bar{N}^2 \tilde{I}_0^*(\vec{\kappa}') \tilde{I}_0(\vec{\kappa}) \langle \tau^*(\vec{\kappa}') \tau(\vec{\kappa}) \rangle_T \\ &\quad + \bar{N} \tilde{I}_0(\vec{\kappa} - \vec{\kappa}') \langle \tau(\vec{\kappa} - \vec{\kappa}') \rangle_T \\ &\quad - \bar{N} \langle \tilde{I}(\vec{\kappa} - \vec{\kappa}') \rangle_T \quad . \end{aligned} \quad (62)$$

Now making use of Eq. (7) to allow us to write

$$\langle \tilde{I}(\vec{\kappa} - \vec{\kappa}') \rangle_T = \tilde{I}_0(\vec{\kappa} - \vec{\kappa}') \langle \tau(\vec{\kappa} - \vec{\kappa}') \rangle_T \quad , \quad (63)$$

we can reduce Eq. (62) to the form

$$\langle S(\vec{\kappa}, \vec{\kappa}') \rangle = \bar{N}^2 \tilde{I}_0^*(\vec{\kappa}') \tilde{I}_0(\vec{\kappa}) \langle \tau^*(\vec{\kappa}') \tau(\vec{\kappa}) \rangle_T \quad . \quad (64)$$

This clearly is an unbiased average containing exactly the form of dependence we expected, i. e., a dependence on the objects spectral amplitudes at spatial frequencies $\bar{\kappa}$ and $\bar{\kappa}'$, and on the turbulence averaged product of the transfer functions at these two spatial frequencies.

We are now ready to ask how accurately does the average of S over a finite series of short exposures approximate the expected value. We expect deviations due to the fact that we have only a finite number of short exposures, thus providing an imperfect average over turbulence, and due to the fact that there are only a finite number of short exposures and a finite number of photon detection events per short exposure, thus providing an imperfect average over the statistics of the photon detection process. These matters are taken up in the next two sections.

3.7 Speckle Interferometry Measurement Accuracy

For evaluation of measurement accuracy in speckle inteferometry we shall be concerned with the quantity

$$\begin{aligned} C_L(\vec{\kappa}, \vec{\kappa}') &= \langle [S(\vec{\kappa}', \vec{\kappa}') - \langle S(\vec{\kappa}', \vec{\kappa}') \rangle]^* [S(\vec{\kappa}, \vec{\kappa}) - \langle S(\vec{\kappa}, \vec{\kappa}) \rangle] \rangle \\ &= \langle S^*(\vec{\kappa}', \vec{\kappa}') S(\vec{\kappa}, \vec{\kappa}) \rangle - \langle S^*(\vec{\kappa}', \vec{\kappa}') \rangle \langle S(\vec{\kappa}, \vec{\kappa}) \rangle . \end{aligned} \quad (65)$$

In Section 9 we shall show exactly how this quantity, $C_L(\vec{\kappa}, \vec{\kappa}')$, is related to the accuracy of a speckle interferometry and will carry out a sample evaluation. In this section we shall be concerned with evaluation of $C_L(\vec{\kappa}, \vec{\kappa}')$ averaged over photon shot noise.

We start our analysis with consideration of the quantity $\langle S^*(\vec{\kappa}', \vec{\kappa}') S(\vec{\kappa}, \vec{\kappa}) \rangle$. Making use of Eq. (59) we can write this as

$$\begin{aligned} \langle S^*(\vec{\kappa}', \vec{\kappa}') S(\vec{\kappa}, \vec{\kappa}) \rangle &= \langle [R^*(\vec{\kappa}') R(\vec{\kappa}') - R^*(0)] \\ &\times [R^*(\vec{\kappa}) R(\vec{\kappa}) - R(0)] \rangle . \end{aligned} \quad (66)$$

It follows from consideration of Eq. 's (21) and (35) [or from consideration of Eq. (37)], that

$$R^*(0) = R(0) . \quad (67)$$

This allows us to rewrite Eq. (66) in the form

$$\begin{aligned} \langle S^*(\vec{\kappa}', \vec{\kappa}') S(\vec{\kappa}, \vec{\kappa}) \rangle &= \langle R^*(\vec{\kappa}') R(\vec{\kappa}') R^*(\vec{\kappa}) R(\vec{\kappa}) \rangle \\ &- \langle R^*(\vec{\kappa}') R(\vec{\kappa}') R(0) \rangle - \langle R^*(\vec{\kappa}) R(\vec{\kappa}) R(0) \rangle \end{aligned}$$

$$+ \langle R(0) R(0) \rangle . \quad (68)$$

In accordance with the notational provisions developed in Section 4, we may make explicit the distinction between the turbulence average and the photon average in Eq. (68). Thus, we write

$$\begin{aligned} \langle S^*(\vec{\kappa}', \vec{\kappa}') S(\vec{\kappa}, \vec{\kappa}) \rangle &= \langle \langle R^*(\vec{\kappa}') R(\vec{\kappa}') R^*(\vec{\kappa}) R(\vec{\kappa}) \rangle_p \rangle_T \\ &- \langle \langle R^*(\vec{\kappa}') R(\vec{\kappa}') R(0) \rangle_p \rangle_T - \langle \langle R^*(\vec{\kappa}) R(\vec{\kappa}) R(0) \rangle_p \rangle_T \\ &+ \langle \langle R(0) R(0) \rangle_p \rangle_T . \end{aligned} \quad (69)$$

Making use of Eq. 's (37) and (38b, c, and d) we can rewrite this as

$$\begin{aligned} \langle S^*(\vec{\kappa}', \vec{\kappa}') S(\vec{\kappa}, \vec{\kappa}) \rangle &= \langle M_4(-\vec{\kappa}', \vec{\kappa}', -\vec{\kappa}, \vec{\kappa}) \rangle_T \\ &- \langle M_3(-\vec{\kappa}', \vec{\kappa}', 0) \rangle_T - \langle M_3(-\vec{\kappa}, \vec{\kappa}, 0) \rangle_T \\ &+ \langle M_2(0, 0) \rangle . \end{aligned} \quad (70)$$

Substituting Eq. 's (45), (50), and (52) into Eq. (70) we get

$$\begin{aligned} \langle S^*(\vec{\kappa}', \vec{\kappa}') S(\vec{\kappa}, \vec{\kappa}) \rangle &= \bar{N}^4 \langle \tilde{I}(-\vec{\kappa}') \tilde{I}(\vec{\kappa}') \tilde{I}(-\vec{\kappa}) \tilde{I}(\vec{\kappa}) \rangle_T \\ &+ \bar{N}^3 \{ \langle \tilde{I}(0) \tilde{I}(-\vec{\kappa}) \tilde{I}(\vec{\kappa}) \rangle_T + \langle \tilde{I}(-\vec{\kappa}' - \vec{\kappa}) \tilde{I}(\vec{\kappa}') \tilde{I}(\vec{\kappa}) \rangle_T \\ &+ \langle \tilde{I}(-\vec{\kappa}' + \vec{\kappa}) \tilde{I}(\vec{\kappa}') \tilde{I}(-\vec{\kappa}) \rangle_T + \langle \tilde{I}(\vec{\kappa}' - \vec{\kappa}) \tilde{I}(-\vec{\kappa}') \tilde{I}(\vec{\kappa}) \rangle_T \\ &+ \langle \tilde{I}(\vec{\kappa}' + \vec{\kappa}) \tilde{I}(-\vec{\kappa}') \tilde{I}(-\vec{\kappa}) \rangle_T + \langle \tilde{I}(0) \tilde{I}(-\vec{\kappa}') \tilde{I}(\vec{\kappa}') \rangle_T \} \\ &+ \bar{N}^2 \{ \langle \tilde{I}(0) \tilde{I}(0) \rangle_T + \langle \tilde{I}(-\vec{\kappa}' - \vec{\kappa}) \tilde{I}(\vec{\kappa}' + \vec{\kappa}) \rangle_T \} \end{aligned}$$

$$\begin{aligned}
& + \langle \tilde{I}(-\vec{\kappa}' + \vec{\kappa}) \tilde{I}(\vec{\kappa}' - \vec{\kappa}) \rangle_{\tau} + \langle \tilde{I}(-\vec{\kappa}) \tilde{I}(\vec{\kappa}) \rangle_{\tau} \\
& + \langle \tilde{I}(\vec{\kappa}) \tilde{I}(-\vec{\kappa}) \rangle_{\tau} + \langle \tilde{I}(-\vec{\kappa}') \tilde{I}(\vec{\kappa}') \rangle_{\tau} + \langle \tilde{I}(\vec{\kappa}') \tilde{I}(-\vec{\kappa}') \rangle_{\tau} \} \\
& + \bar{N} \langle \tilde{I}(0) \rangle_{\tau} \\
& - \bar{N}^3 \langle \tilde{I}(-\vec{\kappa}') \tilde{I}(\vec{\kappa}') \tilde{I}(0) \rangle_{\tau} \\
& - \bar{N}^3 \{ \langle \tilde{I}(0) \tilde{I}(0) \rangle_{\tau} + \langle \tilde{I}(-\vec{\kappa}') \tilde{I}(\vec{\kappa}') \rangle_{\tau} + \langle \tilde{I}(\vec{\kappa}') \tilde{I}(-\vec{\kappa}') \rangle_{\tau} \} \\
& - \bar{N} \langle \tilde{I}(0) \rangle_{\tau} \\
& - \bar{N}^3 \langle \tilde{I}(-\vec{\kappa}) \tilde{I}(\vec{\kappa}) \tilde{I}(0) \rangle_{\tau} \\
& - \bar{N}^3 \{ \langle \tilde{I}(0) \tilde{I}(0) \rangle_{\tau} + \langle \tilde{I}(-\vec{\kappa}) \tilde{I}(\vec{\kappa}) \rangle_{\tau} + \langle \tilde{I}(\vec{\kappa}) \tilde{I}(-\vec{\kappa}) \rangle_{\tau} \} \\
& - \bar{N} \langle \tilde{I}(0) \rangle_{\tau} \\
& + \bar{N}^3 \langle \tilde{I}(0) \tilde{I}(0) \rangle_{\tau} + \bar{N} \langle \tilde{I}(0) \rangle_{\tau} . \tag{71}
\end{aligned}$$

A large number of the terms in Eq. (70) cancel so that the expression can be reduced to the form

$$\begin{aligned}
\langle S^*(\vec{\kappa}', \vec{\kappa}') S(\vec{\kappa}, \vec{\kappa}) \rangle &= \bar{N}^4 \langle \tilde{I}(-\vec{\kappa}') \tilde{I}(\vec{\kappa}') \tilde{I}(-\vec{\kappa}) \tilde{I}(\vec{\kappa}) \rangle_{\tau} \\
&+ \bar{N}^3 \{ \langle \tilde{I}(-\vec{\kappa}' - \vec{\kappa}) \tilde{I}(\vec{\kappa}') \tilde{I}(\vec{\kappa}) \rangle_{\tau} + \langle \tilde{I}(-\vec{\kappa}' + \vec{\kappa}) \tilde{I}(\vec{\kappa}') \tilde{I}(\vec{\kappa}) \rangle_{\tau} \} \\
&+ \langle \tilde{I}(\vec{\kappa}' - \vec{\kappa}) \tilde{I}(-\vec{\kappa}') \tilde{I}(\vec{\kappa}) \rangle_{\tau} + \langle \tilde{I}(\vec{\kappa}' + \vec{\kappa}) \tilde{I}(-\vec{\kappa}') \tilde{I}(-\vec{\kappa}) \rangle_{\tau} \} \\
&+ \bar{N}^3 \{ \langle \tilde{I}(-\vec{\kappa}' - \vec{\kappa}) \tilde{I}(\vec{\kappa}' + \vec{\kappa}) \rangle_{\tau} + \langle \tilde{I}(-\vec{\kappa}' + \vec{\kappa}) \tilde{I}(\vec{\kappa}' - \vec{\kappa}) \rangle_{\tau} \} . \tag{72}
\end{aligned}$$

Making use of Eq. (7) to allow further reduction of Eq. (72), and then combining that result with that of Eq. (64), we can now rewrite Eq. (65) as

$$\begin{aligned}
C_L(\vec{r}, \vec{r}') &= \bar{N}^4 |\tilde{I}_0(\vec{r}')|^2 |\tilde{I}_0(\vec{r})|^2 \{ \langle |\tau(\vec{r}')|^2 |\tau(\vec{r})|^2 \rangle_T \\
&\quad - \langle |\tau(\vec{r}')|^2 \rangle_T \langle |\tau(\vec{r})|^2 \rangle_T \} \\
&\quad + \bar{N}^3 \{ \tilde{I}_0^*(\vec{r}' + \vec{r}) \tilde{I}_0(\vec{r}') \tilde{I}_0(\vec{r}) \langle \tau^*(\vec{r}' + \vec{r}) \tau(\vec{r}') \tau(\vec{r}) \rangle_T \\
&\quad + \tilde{I}_0^*(\vec{r}' - \vec{r}) \tilde{I}_0(\vec{r}') \tilde{I}_0^*(\vec{r}) \langle \tau^*(\vec{r}' - \vec{r}) \tau(\vec{r}') \tau^*(\vec{r}) \rangle_T \\
&\quad + \tilde{I}_0(\vec{r}' + \vec{r}) \tilde{I}_0^*(\vec{r}') \tilde{I}_0^*(\vec{r}) \langle \tau(\vec{r}' + \vec{r}) \tau^*(\vec{r}') \tau^*(\vec{r}) \rangle_T \} \\
&\quad + \bar{N}^2 \{ |\tilde{I}_0(\vec{r}' + \vec{r})|^2 \langle |\tau(\vec{r}' + \vec{r})|^2 \rangle_T \\
&\quad + |\tilde{I}_0(\vec{r}' - \vec{r})|^2 \langle |\tau(\vec{r}' - \vec{r})|^2 \rangle_T \} . \tag{73}
\end{aligned}$$

With this result in hand we are now ready to consider the averages over the turbulence statistics. This is taken up in the next section.

3.8 Averaging Over Turbulence

For our purposes here it will be sufficient to use approximate results for the turbulence averages. As a practical matter we may further restrict our attention to values of $\vec{\kappa}$ and $\vec{\kappa}'$ that are much larger than r_0/λ . Accordingly, we may make use of the approximation^{9,10}

$$\langle |\tau(\vec{\kappa})|^2 \rangle_T \approx 0.435 (r_0/D)^2 \tau_{DL}(\vec{\kappa}) \quad , \quad (74)$$

where r_0 is the turbulence limited coherence diameter, D is the telescope aperture diameter*, and τ_{DL} is the diffraction limited modulation transfer function associated with the aperture. For the case where $\vec{\kappa}' \approx \vec{\kappa}$ then since $|\vec{\kappa}' - \vec{\kappa}|$ can be very small we must write

$$\langle |\tau(\vec{\kappa}' - \vec{\kappa})|^2 \rangle_T \approx |\tau_{DL}(\vec{\kappa}' - \vec{\kappa})|^2 \exp\{-6.88 [|\vec{\kappa}' - \vec{\kappa}|/(k r_0)]^{5/3}\} \quad ,$$

for $\vec{\kappa}' \approx \vec{\kappa}$, (75)

where $k = 2\pi/\lambda$. To accommodate both the case where $\vec{\kappa}' \approx \vec{\kappa}$, and the case where they are significantly unequal, we write, combining Eq.'s (74) and (75)

$$\langle |\tau(\vec{\kappa}' - \vec{\kappa})|^2 \rangle_T \approx |\tau_{DL}(\vec{\kappa}' - \vec{\kappa})|^2 \exp\{-6.88 [|\vec{\kappa}' - \vec{\kappa}|/(k r_0)]^{5/3}\} \\ + 0.435 (r_0/D)^2 \tau_{DL}(\vec{\kappa}' - \vec{\kappa}) \quad . \quad (76)$$

We argue that $\tau(\vec{\kappa})$ is approximately a zero mean gaussian random variable so that odd moments will vanish. Accordingly, we may write

* We assume here a circular clear aperture.

$$\langle \tau^*(\vec{k}' + \vec{k}) \tau(\vec{k}') \tau(\vec{k}) \rangle_T \approx 0 \quad , \quad (77a)$$

$$\langle \tau^*(\vec{k}' - \vec{k}) \tau(\vec{k}') \tau^*(\vec{k}) \rangle_T \approx 0 \quad , \quad (77b)$$

$$\langle \tau(\vec{k}' - \vec{k}) \tau^*(\vec{k}') \tau(\vec{k}) \rangle_T \approx 0 \quad , \quad (77c)$$

$$\langle \tau(\vec{k}' + \vec{k}) \tau^*(\vec{k}') \tau^*(\vec{k}) \rangle_T \approx 0 \quad . \quad (77d)$$

Finally we argue that since $\tau(\vec{k})$ is a zero mean gaussian random variable the fourth moment of its magnitude should be equal to twice the square of the second moment, i. e. ,

$$\langle |\tau(\vec{k})|^4 \rangle_T = 2 [\langle |\tau(\vec{k})|^2 \rangle_T]^2 \quad . \quad (78)$$

Thus, if \vec{k}' and \vec{k} are nearly equal, so that $\tau(\vec{k}')$ and $\tau(\vec{k})$ are well correlated, we expect

$$\langle |\tau(\vec{k}')|^2 |\tau(\vec{k})|^2 \rangle_T \approx 2 \langle |\tau(\vec{k}')|^2 \rangle_T \langle |\tau(\vec{k})|^2 \rangle_T \quad ,$$

$$\text{for } \vec{k}' \approx \vec{k} \quad . \quad (79)$$

On the other hand for \vec{k}' and \vec{k} significantly different in value, so that $\tau(\vec{k}')$ and $\tau(\vec{k})$ are effectively uncorrelated we get

$$\langle |\tau(\vec{k}')|^2 |\tau(\vec{k})|^2 \rangle_T \approx \langle |\tau(\vec{k}')|^2 \rangle_T \langle |\tau(\vec{k})|^2 \rangle_T \quad ,$$

$$\text{for } \vec{k}' \neq \vec{k} \quad . \quad (80)$$

Based on the information we have¹⁰ on the way the correlation between $\tau(\vec{k}')$ and $\tau(\vec{k})$ decreases with increasing value of $|\vec{k}' - \vec{k}|$, we argue

that a reasonable form, interpolating between the results of Eq. 's (79) and (80) is

$$\begin{aligned} \langle |\tau(\vec{\kappa}')|^2 |\tau(\vec{\kappa})|^2 \rangle_T &\approx \langle |\tau(\vec{\kappa}')|^2 \rangle_T \langle |\tau(\vec{\kappa})|^2 \rangle_T \\ &\times \left(1 + \exp\{-6.88[|\vec{\kappa}' - \vec{\kappa}|/(k r_0)]^{5/3}\} \right). \end{aligned} \quad (81)$$

Making use of Eq. 's (74), (76), (77), and (81) we can now rewrite Eq. (73) as

$$\begin{aligned} C_L(\vec{\kappa}, \vec{\kappa}') &= \bar{N}^4 |\tilde{I}_0(\vec{\kappa}')|^2 |\tilde{I}_0(\vec{\kappa})|^2 (0.435)^2 (r_0/D)^4 \tau_{DL}(\vec{\kappa}') \tau_{DL}(\vec{\kappa}) \\ &\times \exp\{-6.88[|\vec{\kappa}' - \vec{\kappa}|/(k r_0)]^{5/3}\} \\ &+ \bar{N}^2 |\tilde{I}_0(\vec{\kappa}' + \vec{\kappa})|^2 (0.435) (r_0/D)^2 \tau_{DL}(\vec{\kappa}' + \vec{\kappa}) \\ &+ \bar{N}^2 |\tilde{I}_0(\vec{\kappa}' - \vec{\kappa})|^2 \{ (0.435) (r_0/D)^2 \tau_{DL}(\vec{\kappa}' - \vec{\kappa}) \\ &+ |\tau_{DL}(\vec{\kappa}' - \vec{\kappa})|^2 \exp\{-6.88[|\vec{\kappa}' - \vec{\kappa}|/(k r_0)]^{5/3}\} \}. \end{aligned} \quad (82)$$

With this result in hand for the covariance of the spectral strength obtained with the Labeyrie method of spectral interferometry, we can calculate the expected error in this process. To make this quantity meaningful we also need an expression for the expected signal strength. We can obtain this from Eq. (64), which in conjunction with Eq. (74) leads to the result that

$$\langle S(\vec{\kappa}, \vec{\kappa}) \rangle = \bar{N}^2 |\tilde{I}_0(\vec{\kappa})|^2 (0.435) (r_0/D)^2 \tau_{DL}(\vec{\kappa}). \quad (83)$$

In the next section we use Eq. (82) and (83) to form an estimate of the accuracy of speckle interferometry measurements.

3.9 Speckle Interferometry Measurement Accuracy

In speckle interferometry we form a set of M statistically independent speckle patterns, and then by fourier transforming and averaging over these M patterns, we develop an estimate of $S(\vec{\kappa}, \vec{\kappa})$. The expected value of this quantity is $\langle S(\vec{\kappa}, \vec{\kappa}) \rangle$, just as given by Eq. (83). The covariance associated with this quantity will be $C_L(\vec{\kappa}, \vec{\kappa}')/M$, with the value of $C_L(\vec{\kappa}, \vec{\kappa}')$ given by Eq. (82). Nominally, this establishes a "signal-to-noise ratio" in the spatial frequency domain, SNR_{κ} , which we can write as

$$SNR_{\kappa} = \langle S(\vec{\kappa}, \vec{\kappa}) \rangle^2 / [C_L(\vec{\kappa}, \vec{\kappa})/M] . \quad (84)$$

Making use of Eq. 's (82) and (83) with appropriate approximations, we can rewrite Eq. (84) as

$$SNR_{\kappa} = \frac{M}{1 + [\bar{N} |\tilde{I}_0(\vec{\kappa})|^2 (0.435)(r_0/D)^2 \tau_{0L}(\vec{\kappa})]^{-2}} , \quad (85)$$

where we have assumed that r_0 is very much less than D . The interpretation of this formula is in a sense straightforward. If the average photon detection events per single short exposure, \bar{N} , is large enough so that $\bar{N} |\tilde{I}_0(\vec{\kappa})|^2 (0.435)(r_0/D)^2 \tau_{0L}(\vec{\kappa})$ is significantly greater than unity, then the signal-to-noise ratio will not be improved by any increase in the photon flux — the process will not be limited by shot noise but rather will be entirely limited by turbulence effects and the need to average over many realizations of the random turbulence effects.

Unfortunately, this spatial frequency domain signal-to-noise ratio, while it is useful in providing us with some insight into the required photon detection event rate is not directly relatable to the accuracy of a measurement quantity of interest. It is measurements in the spatial (rather than

the spatial frequency) domain that are basically of interest to us. It is in terms of the evaluation of this type of quantity that we wish to determine the measurement accuracy and the associated signal-to-noise ratio. As an example of this we consider the observation of a binary star pair. We consider a binary star pair with an angular separation $\bar{\theta}$ and with an intensity ratio ρ (with ρ less than unity). As an example to be pursued here, we ask how accurately we can determine the value of ρ with a set of M short exposure photographs if there are an average of $\bar{N}(1 + \rho)$ detected photon events per short exposure.

For this pair of binary stars, making use of Eq. 's (2) and (3) we can see that

$$I_0(\bar{r}) = (1 + \rho)^{-1} [\delta(\bar{r}) + \rho \delta(\bar{r} - \bar{\theta})] \quad , \quad (86)$$

so that

$$\tilde{I}_0(\bar{\kappa}) = (1 + \rho)^{-1} [1 + \rho \exp(-i \bar{\kappa} \cdot \bar{\theta})] \quad . \quad (87)$$

A set of M short exposures will be used to form the quantity $\bar{S}(\bar{\kappa})$ which estimates $\langle S(\bar{\kappa}, \bar{\kappa}) \rangle$. For observation of turbulence statistics, based most likely on images of a bright single star, a normalization factor $s_N(\bar{\kappa})$ will be formed, which will have a nominal value of

$$s_N(\bar{\kappa}) = 0.435 (r_0/D)^2 \tau_{0L}(\bar{\kappa}) \quad , \quad (88)$$

for large values of $|\bar{\kappa}|$, but actually corresponding everywhere to the basic modulation transfer function of the speckle interferometry process.

The basic speckle interferometry process would proceed by forming the ratio $\bar{S}(\bar{\kappa})/s_N(\bar{\kappa})$, which in accordance with Eq. (83) and (87) should approximate the power spectrum of the binary star image, i. e.,

$$\bar{S}(\vec{\kappa})/s_N(\vec{\kappa}) \approx \bar{N}^2 |\tilde{I}_0(\vec{\kappa})|^2 . \quad (89)$$

Making use of Eq. (87) this takes the form

$$\bar{S}(\vec{\kappa})/s_N(\vec{\kappa}) \approx \bar{N}^2 (1 + \rho)^{-2} [1 + \rho^2 + 2\rho \cos(\vec{\kappa} \cdot \vec{\theta})] . \quad (90)$$

This quantity would then be fourier transformed to form an estimate of the correlation function associated with the binary star pair's image.

We obtain for the correlation function

$$\mathcal{J}(\vec{r}) = (2\pi)^{-2} \int d\vec{\kappa} \exp(i \vec{\kappa} \cdot \vec{r}) \bar{S}(\vec{\kappa})/s_N(\vec{\kappa}) . \quad (91)$$

If we substitute Eq. (90) into Eq. (91) and carry out the fourier transformation integration we get as the nominal correlation function

$$\mathcal{J}(\vec{r}) = \bar{N}^2 (1 + \rho)^{-2} [(1 + \rho^2) \delta(\vec{r}) + \rho \delta(\vec{r} - \vec{\theta}) + \rho \delta(\vec{r} + \vec{\theta})] , \quad (92)$$

which is exactly the correlation function we would expect for the binary star pair's image — a main lobe of relative strength $1 + \rho^2$ at the origin, and two side lobes, each of relative strength ρ at displacements of $\pm \vec{\theta}$. In writing Eq. (92) we have used the equivalence

$$\delta(\vec{r}) = (2\pi)^{-2} \int d\vec{\kappa} \exp(i \vec{\kappa} \cdot \vec{r}) . \quad (93)$$

Since the main lobe and side lobes can be separately measured we can form the ratio \mathcal{R} whose nominal value is

$$\mathcal{R} \approx \rho / (1 + \rho^2) , \quad (94)$$

but whose measured value is $\bar{R} = R + \delta R$. This allows us to calculate the relative intensity of the two binary stars.

Solving for ρ we get

$$\rho = \frac{1 + (1 - 4R^2)^{1/2}}{2R} . \quad (95)$$

Our basic concern is with the effect of some fractional error

$$\epsilon = \delta R / R , \quad (96)$$

in the actual determination of \bar{R} (due to the statistical nature of the speckle interferometry process) on the fractional error

$$\mu = \delta \rho / \rho , \quad (97)$$

in the determination of the relative intensity, ρ , of the pair of binary stars. To obtain this relationship we write, in accordance with Eq. (95), that

$$\rho + \delta \rho = \frac{1 + [1 - 4(R + \delta R)^2]^{1/2}}{2(R + \delta R)} . \quad (98)$$

This can be rewritten as

$$\rho + \delta \rho = \frac{1 + [1 - 4R^2(1 + \epsilon)^2]^{1/2}}{2R(1 + \epsilon)} , \quad (99)$$

which we can approximate, for ϵ small, by the expression

$$\begin{aligned}
\rho(1 + \mu) &\approx \frac{1 + \sqrt{(1 - 4R^2) \{1 - [4R^2/(1 - 4R^2)](2\epsilon)\}}}{2R(1 + \epsilon)} \\
&\approx \frac{1 + (1 - 4R^2)^{1/2} \{1 - \frac{1}{2}[4R^2/(1 - 4R^2)](2\epsilon)\}}{2R(1 + \epsilon)} \\
&\approx \frac{1 + (1 - 4R^2)^{1/2}}{2R} - \frac{2R}{(1 - 4R^2)^{1/2}} \epsilon - \frac{1 + (1 - 4R^2)^{1/2}}{2R} \epsilon^2. \quad (100)
\end{aligned}$$

(Of course, this approximation breaks down when $\rho \approx 1$, and $R \approx \frac{1}{2}$.)
 Making use of Eq. (95) we can reduce this expression to the form

$$\rho \mu = - \frac{1 + (1 - 4R^2)^{1/2}}{2R(1 - 4R^2)^{1/2}} \epsilon, \quad (101)$$

so that finally we get

$$\mu = - \frac{\epsilon}{(1 - 4R^2)^{1/2}}. \quad (102)$$

Eq. (102) allows us to relate the fractional error in the measurement of the ratio of the magnitude of the two correlation peaks of a binary star pair's correlation pattern to the ratio of the intensity of the two stars. Our problem is thus one of estimating how accurately we can measure the ratio $\bar{R} = R + \delta R$ for the correlation peaks.

To see how well this ratio can be determined, we note that in accordance with Eq. (92) we can write for the measured ratio

$$\begin{aligned}
\bar{R} &= R + \delta R \\
&= \mathcal{J}(\bar{\theta})/\mathcal{J}(0). \quad (103)
\end{aligned}$$

Making use of Eq. (91) and noting that since $\bar{S}(\bar{\kappa})$ estimates $\langle S(\bar{\kappa}, \bar{\kappa}) \rangle$,

then the value of \mathcal{R} is obtained when $\bar{S}(\vec{\kappa})$ in Eq. (91) is replaced by $\langle S(\vec{\kappa}, \vec{\kappa}) \rangle$, and that substituted into Eq. (92), we see that we can write

$$\begin{aligned} \delta \mathcal{R} = & \frac{(2\pi)^{-2} \int d\vec{\kappa} \exp(i \vec{\kappa} \cdot \vec{\theta}) [\bar{S}(\vec{\kappa}) - \langle S(\vec{\kappa}, \vec{\kappa}) \rangle] / s_N(\vec{\kappa})}{(2\pi)^{-2} \int d\vec{\kappa} \langle S(\vec{\kappa}, \vec{\kappa}) \rangle / s_N(\vec{\kappa})} \\ & - \frac{(2\pi)^{-2} \int d\vec{\kappa} \exp(i \vec{\kappa} \cdot \vec{\theta}) \langle S(\vec{\kappa}, \vec{\kappa}) \rangle / s_N(\vec{\kappa})}{(2\pi)^{-2} \int d\vec{\kappa} \langle S(\vec{\kappa}, \vec{\kappa}) \rangle / s_N(\vec{\kappa})} \\ & \times \frac{(2\pi)^{-2} \int d\vec{\kappa} [\bar{S}(\vec{\kappa}) - \langle S(\vec{\kappa}, \vec{\kappa}) \rangle] / s_N(\vec{\kappa})}{(2\pi)^{-2} \int d\vec{\kappa} \langle S(\vec{\kappa}, \vec{\kappa}) \rangle / s_N(\vec{\kappa})} . \end{aligned} \quad (104)$$

We note that since $s_N(\vec{\kappa})$ is a normalization function chosen to everywhere correspond to the speckle process's transfer function, then in accordance with Eq. (83), [and taking note of Eq. (88)], we can write

$$\begin{aligned} \int d\vec{\kappa} \langle S(\vec{\kappa}, \vec{\kappa}) \rangle / s_N(\vec{\kappa}) &= N^2 \int d\vec{\kappa} |\tilde{I}_0(\vec{\kappa})|^2 \\ &= N^2 C . \end{aligned} \quad (105)$$

It is easy to see from consideration of Eq. (87) that

$$\begin{aligned} C &= \int d\vec{\kappa} |\tilde{I}_0(\vec{\kappa})|^2 \\ &= (1 + \rho)^{-2} \int d\vec{\kappa} |1 + \rho \exp(-i \vec{\kappa} \cdot \vec{\theta})|^2 \\ &\approx [(1 + \rho^2)/(1 + \rho)^2] \pi (kD)^2 , \end{aligned} \quad (106)$$

where the factor of $\pi (kD)^2$ appears here as a consequence of the fact that the range of the $\vec{\kappa}$ -integration is a circle within which $|\vec{\kappa}| < kD$, i. e.,

less than the diffraction limited transfer function cut-off spatial frequency, kD^* . Noting that

$$R = \frac{(2\pi)^{-2} \int d\vec{k} \exp(i \vec{k} \cdot \vec{\theta}) \langle S(\vec{k}, \vec{k}) \rangle / s_N(\vec{k})}{(2\pi)^{-2} \int d\vec{k} \langle S(\vec{k}, \vec{k}) \rangle / s_N(\vec{k})}, \quad (107)$$

we can now write in place of Eq. (104)

$$\epsilon = (\bar{N}^2 C R)^{-1} \int d\vec{k} \left[\frac{\exp(i \vec{k} \cdot \vec{\theta}) - R}{s_N(\vec{k})} \right] [\bar{S}(\vec{k}) - \langle S(\vec{k}, \vec{k}) \rangle]. \quad (108)$$

Our interest is in the evaluation of the mean square value of the fractional error in ϵ , the measurement of the ratio of the two peaks in the correlation function.

$$\begin{aligned} \sigma_\epsilon^2 &= \langle |\epsilon|^2 \rangle \\ &= (\bar{N}^2 C R)^{-2} \iint d\vec{k} d\vec{k}' \left[\frac{\exp(-i \vec{k}' \cdot \vec{\theta}) - R^*}{s_N^*(\vec{k}')} \right] \left[\frac{\exp(i \vec{k} \cdot \vec{\theta}) - R}{s_N(\vec{k})} \right] \\ &\quad \times \langle [\bar{S}(\vec{k}') - \langle S(\vec{k}', \vec{k}') \rangle]^* [\bar{S}(\vec{k}) - \langle S(\vec{k}, \vec{k}) \rangle] \rangle. \end{aligned} \quad (109)$$

In as much as $\bar{S}(\vec{k})$ is the measurement approximation to $S(\vec{k}, \vec{k})$ except averaged over M short exposures, then we can replace the ensemble average in Eq. (109) by $C_L(\vec{k}, \vec{k}')/M$, where C_L is defined initially in Eq. (65), and in the form we shall use in Eq. (82). This allows us to write

$$\begin{aligned} \sigma_\epsilon^2 &= (\bar{N}^2 C R)^{-2} M^{-1} \iint d\vec{k} d\vec{k}' \left[\frac{\exp(-i \vec{k}' \cdot \vec{\theta}) - R^*}{s_N^*(\vec{k}')} \right] \left[\frac{\exp(i \vec{k} \cdot \vec{\theta}) - R}{s_N(\vec{k})} \right] \\ &\quad \times \left\{ \bar{N}^4 |\tilde{I}_0(\vec{k}')|^2 |\tilde{I}_0(\vec{k})|^2 (0.435)^2 (r_0/D)^4 \tau_{0L}(\vec{k}') \tau_{0L}(\vec{k}) \right\} \end{aligned}$$

* Assuming $\theta > \lambda/D$ we have dropped a term of the order of $\rho J_1(2\pi\theta D/\lambda)/(2\pi\theta D/\lambda)$ in Eq. (106).

$$\begin{aligned}
& \times \exp \{-6.88 [|\vec{\kappa}' - \vec{\kappa}| / (k r_0)]^{5/3}\} \\
& + N^2 |\tilde{I}_0(\vec{\kappa}' + \vec{\kappa})|^2 (0.435)(r_0/D)^2 \tau_{0L}(\vec{\kappa} + \vec{\kappa}') \\
& + N^2 |\tilde{I}_0(\vec{\kappa} - \vec{\kappa}')|^2 [(0.435)(r_0/D)^2 \tau_{0L}(\vec{\kappa}' - \vec{\kappa}) \\
& + |\tau_{0L}(\vec{\kappa} - \vec{\kappa}')|^2 \exp \{-6.88 [|\vec{\kappa} - \vec{\kappa}'| / (k r_0)]^{5/3}\}] \}. \quad (110)
\end{aligned}$$

Making use of Eq. (88) we rewrite this in the form

$$\begin{aligned}
\sigma_s^2 &= (C^2 R^2 M)^{-1} \iint d\vec{\kappa} d\vec{\kappa}' [\exp(-i \vec{\kappa}' \cdot \vec{\theta}) - R^*] [\exp(i \vec{\kappa} \cdot \vec{\theta}) - R] \\
&\times \left\{ |\tilde{I}_0(\vec{\kappa}')|^2 |\tilde{I}_0(\vec{\kappa})|^2 \exp[-6.88 [|\vec{\kappa}' - \vec{\kappa}| / (k r_0)]^{5/3}] \right. \\
&+ \frac{|\tilde{I}_0(\vec{\kappa} + \vec{\kappa}')|^2 \tau_{0L}(\vec{\kappa} + \vec{\kappa}')}{N^2 (0.435)(r_0/D)^2 \tau_{0L}(\vec{\kappa}) \tau_{0L}(\vec{\kappa}')} \\
&+ \frac{|\tilde{I}_0(\vec{\kappa} - \vec{\kappa}')|^2 \tau_{0L}(\vec{\kappa} - \vec{\kappa}')}{N^2 (0.435)(r_0/D)^2 \tau_{0L}(\vec{\kappa}) \tau_{0L}(\vec{\kappa}')} \\
&\left. + \frac{|\tilde{I}_0(\vec{\kappa} - \vec{\kappa}')|^2 |\tau_{0L}(\vec{\kappa} - \vec{\kappa}')|^2 \exp[-6.88 [|\vec{\kappa} - \vec{\kappa}'| / (k r_0)]^{5/3}]}{N^2 (0.435)^2 (r_0/D)^4 \tau_{0L}(\vec{\kappa}) \tau_{0L}(\vec{\kappa}')} \right\}. \quad (111)
\end{aligned}$$

In these integrations, though it is not explicitly stated, it is to be understood that the integration range only includes values of $\vec{\kappa}$ and $\vec{\kappa}'$ for which the diffraction limited transfer function, τ_{0L} , does not vanish.

Rather than attempt to exactly evaluate the multiple integral in Eq. (111) it is convenient to approximate the result in the two limiting cases of 1) very large photon flux, i. e., \bar{N} very large, and 2) a very weak photon flux, i. e., \bar{N} very small. For the first case we can write

$$\begin{aligned} \sigma_{e,1}^2 &= \sigma_e^2, \text{ for } \bar{N} \gg 1 \\ &\approx (C^2 \mathcal{R}^2 M)^{-1} \iint d\vec{\kappa} d\vec{\kappa}' [\exp(-i \vec{\kappa}' \cdot \vec{\theta}) - \mathcal{R}^*] [\exp(i \vec{\kappa} \cdot \vec{\theta}) - \mathcal{R}] \\ &\quad \times |I_0(\vec{\kappa}')|^2 |I_0(\vec{\kappa})|^2 \exp\{-6.88[|\vec{\kappa}' - \vec{\kappa}|/(k r_0)]^{5/3}\}. \end{aligned} \quad (112)$$

If we now make use of Eq. (87) and furthermore, restrict our attention to the case of binary star pairs whose angular separation, $|\vec{\theta}|$, is too small to be resolved by conventional imagery, i. e.,

$$|\vec{\theta}| \ll (k r_0)^{-1}, \quad (113)$$

then we can make the approximation that

$$\begin{aligned} \sigma_{e,1}^2 &\approx (C^2 \mathcal{R}^2 M)^{-1} [\pi(k D)^2] \left[\frac{1 + \rho^2}{(1 + \rho)^2} \right]^2 (1 - \mathcal{R}^2) \\ &\quad \times \int d\vec{u} \exp\{-6.88[|\vec{u}|/(k r_0)]^{5/3}\}. \end{aligned} \quad (114)$$

It can be shown that

$$\begin{aligned} \int d\vec{u} \exp\{-6.88[|\vec{u}|/(k r_0)]^{5/3}\} &= 2\pi [(6.88)^{-3/5} k r_0]^2 \\ &\quad \times \int_0^\infty v dv \exp(-v^{5/3}) \\ &= 0.6211 (k r_0)^2 \frac{3}{8} \int_0^\infty x^{1/5} \exp(-x) dx \end{aligned}$$

$$\begin{aligned}
&= 0.3726 (k r_0)^2 \Gamma(6/5) \\
&= 0.3422 (k r_0)^2 .
\end{aligned} \tag{115}$$

Now making use of Eq. 's (95) and (106) to provide values for \mathcal{R} and C , respectively, and using Eq. (115), we can reduce Eq. (114) to the form

$$\sigma_{\epsilon,1}^2 \approx \frac{0.1089}{M} (r_0/D)^2 \left(\frac{2\rho - \rho^2 + 2\rho^3}{\rho^2} \right) . \tag{116}$$

Making use of Eq. 's (102) and (95) we can see that in this case the rms error in the measurement of the ratio will be

$$\begin{aligned}
\sigma_{\rho,1}^2 &= \rho^2 \langle \mu_1^2 \rangle \\
&= \rho^2 \sigma_{\mu,1}^2 \\
&= \rho^2 \frac{\sigma_{\epsilon,1}^2}{(1-4\mathcal{R}^2)^{1/2}} \\
&= \rho^2 \left(\frac{1+\rho^2}{1-\rho^2} \right) \left(\frac{2\rho - \rho^2 + 2\rho^3}{\rho^2} \right) (0.1089)(r_0/D)^2/M \\
&= (2\rho - \rho^2 + 2\rho^3) \left(\frac{1+\rho^2}{1-\rho^2} \right) (0.1089)(r_0/D)^2/M .
\end{aligned} \tag{117}$$

This represents our basic result for our ability to measure the relative intensity of a pair of (unequal intensity) binary stars for case 1, when the photon flux rate is very high and the error is associated with the imperfect average over turbulence effects provided by M short exposures.

For case 2, where the photon flux rate is very low we can approximate $\sigma_{\epsilon,2}^2$ as given in Eq. (111) by the expression

$$\begin{aligned} \sigma_{\epsilon,2}^2 &\approx (C^2 R^2 M)^{-1} \iint d\vec{\kappa} d\vec{\kappa}' [\exp(-i \vec{\kappa}' \cdot \vec{\theta}) - R^*] [\exp(i \vec{\kappa} \cdot \vec{\theta}) - R] \\ &\quad \times \frac{|\tilde{I}_0(\vec{\kappa} + \vec{\kappa}')|^2 \tau_{DL}(\vec{\kappa} + \vec{\kappa}') + |\tilde{I}_0(\vec{\kappa} - \vec{\kappa}')|^2 \tau_{DL}(\vec{\kappa} - \vec{\kappa}')}{N^2 (0.435) (r_0/D)^2 \tau_{DL}(\vec{\kappa}) \tau_{DL}(\vec{\kappa}')} \\ &\approx 2(C^2 R^2 M)^{-1} \iint d\vec{\kappa} d\vec{\kappa}' R^2 \frac{|\tilde{I}_0(\vec{\kappa} - \vec{\kappa}')|^2 \tau_{DL}(\vec{\kappa} - \vec{\kappa}')}{N^2 (0.435) (r_0/D)^2 \tau_{DL}(\vec{\kappa}) \tau_{DL}(\vec{\kappa}')} . \end{aligned} \quad (118)$$

Making use of Eq. (87) and approximating the diffraction limited transfer function τ_{DL} , (whose value varies from 1 to 0) by the constant $\frac{1}{3}$, we can approximate

$$\sigma_{\epsilon,2}^2 \approx 2(C^2 M)^{-1} \frac{[(1+\rho^2)/(1+\rho)^2]^{\frac{1}{3}} [\pi (kD)^2]^2}{N^2 (0.435) (r_0/D)^2 (\frac{1}{3})^2} . \quad (119)$$

Now making use of Eq. 's (95) and (106) we can reduce this expression to the form

$$\sigma_{\epsilon,2}^2 \approx \frac{13.8}{MN^2} \left(\frac{D}{r_0}\right)^2 \frac{(1+\rho)^2}{(1+\rho^2)} . \quad (120)$$

Following the procedure of Eq. (117) we see that in this case the rms error in our measurement of the ratio of the intensity of the two stars in the binary star pair will be

$$\sigma_{\rho,2}^2 = \rho^2 \frac{\sigma_{\epsilon,2}^2}{(1-4R^2)\mu^2}$$

$$\begin{aligned}
&= \rho^2 \frac{1 + \rho^2}{1 - \rho^2} \left\{ \frac{13.8}{M \bar{N}^2} \left(\frac{D}{r_0} \right)^2 \frac{(1 + \rho)^2}{(1 + \rho^2)} \right\} \\
&= \frac{13.8}{M \bar{N}^2} \left(\frac{D}{r_0} \right)^2 \frac{1 + \rho}{1 - \rho} \rho^2 \quad . \quad (121)
\end{aligned}$$

It is interesting to note here that since \bar{N} is proportional to D^2 , increasing the aperture area will reduce the rms error in our measured value of ρ , but only as the first power of the aperture diameter.

It is convenient to combine our results for the two limiting cases of a very large photon flux rate and of a very low photon flux rate, writing

$$\begin{aligned}
\sigma_{\rho^2} &= \sigma_{\rho^2,1}^2 + \sigma_{\rho^2,2}^2 \\
&= \frac{0.1089}{M} \left(\frac{r_0}{D} \right)^2 (2\rho - \rho^2 + 2\rho^3) \left(\frac{1 + \rho^2}{1 - \rho^2} \right) \\
&\quad + \frac{13.8}{M \bar{N}^2} \left(\frac{D}{r_0} \right)^2 \frac{1 + \rho}{1 - \rho} \rho^2 \quad . \quad (122)
\end{aligned}$$

With this result established we are now ready to consider the magnitude of noise effects in the Knox-Thompson speckle imagery technique. We take this up in the following sections.

3.10 Accuracy of Speckle Imagery

For consideration of noise effects in speckle imagery our basic concern is with error in the estimation of $\langle S(\vec{\kappa}, \vec{\kappa}') \rangle$ for $\vec{\kappa}'$ approximately but not exactly equal to $\vec{\kappa}$. In the speckle imagery process the phase of $\langle S(\vec{\kappa}, \vec{\kappa}') \rangle$ is determined for an array of values of $\vec{\kappa}$ and $\vec{\kappa}'$ that "cover" the $\vec{\kappa}$ -space range of interest. These phase values may be considered to be equal to the difference in the phase shift associated with the image pattern's spatial frequency components $\tilde{I}_0(\vec{\kappa})$ and $\tilde{I}_0(\vec{\kappa}')$. By a least square method these phase differences are then combined so as to span the entire spatial frequency domain, yielding the (absolute) phase shift to be associated with each spatial frequency component in image patterns spectrum, $\tilde{I}_0(\vec{\kappa})$. It can be shown¹¹ that if the mean square error in the determination of the phase difference is constant over the spatial frequency domain, and is equal to $\sigma_{\Delta\varphi}^2$, then the mean square error in the calculated phase will be

$$\sigma_{\varphi}^2 \approx \frac{2}{3} \left[1 + \frac{1}{4} \ln(N) \right] \sigma_{\Delta\varphi}^2, \quad (123)$$

where N is the number of points in the spatial frequency domain on which the phase is to be determined, and over adjacent pairs of which the phase difference is measured. Knowing the values of $\sigma_{\Delta\varphi}^2$, the mean square phase difference, and of N , the number of measurement points in the spatial frequency domains, we can then consider the mean square error in our knowledge of the phase of each of image spatial frequency components, σ_{φ}^2 , to be known. We may take σ_{φ}^2 as a measure of the quality of the speckle imagery ultimately recovered, nominally estimating the effective resolution as

$$R_{s1} = \exp(-\sigma_{\varphi}^2). \quad (124)$$

This may be considered to be a measure of the Strehl definition of the recovered image relative to the ideal diffraction limited image.

Our immediate concern is with the evaluation of $\sigma_{\Delta\varphi}^2$. We take this up in Section 3.11, recognizing that the measured phase difference is actually a function of \vec{k} , and so busy ourselves there with calculating $\sigma_{\Delta\varphi}^2(\vec{k})$. In Section 3.12 we introduce consideration of the entire spatial frequency domain, and evaluating \mathfrak{N} , so that we can then determine σ_{φ}^2 and \mathcal{R}_{s1} . We shall develop both of these quantities in Section 3.12.

3.11 Speckle Imagery Phase Difference Error

The starting point for our calculations here is our ability to evaluate $\langle |S(\vec{\kappa}, \vec{\kappa}')|^2 \rangle$. From this we can evaluate the mean square error contained in our estimate of $\langle S(\vec{\kappa}, \vec{\kappa}') \rangle$ as formed from M frames. Since $S(\vec{\kappa}, \vec{\kappa}')$ is a complex number the error is as likely to be in the real part as in the imaginary part — or put in more relevant terms, as likely to be parallel to $\langle S(\vec{\kappa}, \vec{\kappa}') \rangle$ as it is to be perpendicular to $\langle S(\vec{\kappa}, \vec{\kappa}') \rangle$ in the complex plane containing $\langle S(\vec{\kappa}, \vec{\kappa}') \rangle$. Thus, based on the assumption that after averaging M frames the error will be small, we can approximate the mean square error in our estimate of the argument of $\langle S(\vec{\kappa}, \vec{\kappa}') \rangle$, which is the mean square phase error, as

$$\sigma_{\Delta\phi}^2(\vec{\kappa}) = M^{-1} \frac{\frac{1}{2}[\langle |S(\vec{\kappa}, \vec{\kappa}')|^2 \rangle - |\langle S(\vec{\kappa}, \vec{\kappa}') \rangle|^2]}{|\langle S(\vec{\kappa}, \vec{\kappa}') \rangle|^2} . \quad (125)$$

Making use of Eq. (59) we can write

$$\begin{aligned} \langle |S(\vec{\kappa}, \vec{\kappa}')|^2 \rangle &= \langle |R^*(\vec{\kappa}') R(\vec{\kappa}) - R(\vec{\kappa} - \vec{\kappa}')|^2 \rangle \\ &= \langle R^*(\vec{\kappa}') R(\vec{\kappa}') R^*(\vec{\kappa}) R(\vec{\kappa}) \rangle \\ &\quad - \langle R^*(\vec{\kappa}') R(\vec{\kappa}) R^*(\vec{\kappa} - \vec{\kappa}') \rangle \\ &\quad - \langle R^*(\vec{\kappa}) R(\vec{\kappa}') R(\vec{\kappa} - \vec{\kappa}') \rangle \\ &\quad + \langle R^*(\vec{\kappa} - \vec{\kappa}') R(\vec{\kappa} - \vec{\kappa}') \rangle . \end{aligned} \quad (126)$$

By exploiting the formalism developed in Section 4 and substituting as appropriate using Eq. 's (37) and (38a, b, c, and d), we can rewrite Eq. (126) as

$$\begin{aligned}
\langle |S(\vec{\kappa}, \vec{\kappa}')|^2 \rangle &= \langle M_4(-\vec{\kappa}', \vec{\kappa}', -\vec{\kappa}, \vec{\kappa}) \rangle_T \\
&- \langle M_3(-\vec{\kappa}', \vec{\kappa}, \vec{\kappa}' - \vec{\kappa}) \rangle_T - \langle M_3(-\vec{\kappa}, \vec{\kappa}', \vec{\kappa} - \vec{\kappa}') \rangle_T \\
&+ \langle M_2(\vec{\kappa}' - \vec{\kappa}, \vec{\kappa} - \vec{\kappa}') \rangle_T .
\end{aligned} \tag{127}$$

Now substituting Eq. 's (45), (50), and (52) into Eq. (127) we can obtain the result that

$$\begin{aligned}
\langle |S(\vec{\kappa}, \vec{\kappa}')|^2 \rangle &= \{ \overline{N}^4 \langle \tilde{I}(-\vec{\kappa}') \tilde{I}(\vec{\kappa}') \tilde{I}(-\vec{\kappa}) \tilde{I}(\vec{\kappa}) \rangle_T \\
&+ \overline{N}^3 \langle \tilde{I}(0) \tilde{I}(-\vec{\kappa}) \tilde{I}(\vec{\kappa}) \rangle_T + \overline{N}^3 \langle \tilde{I}(-\vec{\kappa}' - \vec{\kappa}) \tilde{I}(\vec{\kappa}') \tilde{I}(\vec{\kappa}) \rangle_T \\
&+ \overline{N}^3 \langle \tilde{I}(\vec{\kappa} - \vec{\kappa}') \tilde{I}(\vec{\kappa}') \tilde{I}(-\vec{\kappa}) \rangle_T + \overline{N}^3 \langle \tilde{I}(\vec{\kappa}' - \vec{\kappa}) \tilde{I}(-\vec{\kappa}') \tilde{I}(\vec{\kappa}) \rangle_T \\
&+ \overline{N}^3 \langle \tilde{I}(\vec{\kappa}' + \vec{\kappa}) \tilde{I}(-\vec{\kappa}') \tilde{I}(-\vec{\kappa}) \rangle_T + \overline{N}^3 \langle \tilde{I}(0) \tilde{I}(-\vec{\kappa}') \tilde{I}(\vec{\kappa}') \rangle_T \\
&+ \overline{N}^2 \langle \tilde{I}(0) \tilde{I}(0) \rangle_T + \overline{N}^2 \langle \tilde{I}(-\vec{\kappa}' - \vec{\kappa}) \tilde{I}(\vec{\kappa}' + \vec{\kappa}) \rangle_T \\
&+ \overline{N}^2 \langle \tilde{I}(\vec{\kappa} - \vec{\kappa}') \tilde{I}(\vec{\kappa}' - \vec{\kappa}) \rangle_T + \overline{N}^2 \langle \tilde{I}(-\vec{\kappa}) \tilde{I}(\vec{\kappa}) \rangle_T \\
&+ \overline{N}^2 \langle \tilde{I}(\vec{\kappa}) \tilde{I}(-\vec{\kappa}) \rangle_T + \overline{N}^2 \langle \tilde{I}(-\vec{\kappa}') \tilde{I}(\vec{\kappa}') \rangle_T \\
&+ \overline{N}^2 \langle \tilde{I}(\vec{\kappa}') \tilde{I}(-\vec{\kappa}') \rangle_T + \overline{N} \langle \tilde{I}(0) \rangle_T \} \\
&- \{ \overline{N}^3 \langle \tilde{I}(-\vec{\kappa}') \tilde{I}(\vec{\kappa}) \tilde{I}(\vec{\kappa}' - \vec{\kappa}) \rangle_T + \overline{N}^2 \langle \tilde{I}(\vec{\kappa} - \vec{\kappa}') \tilde{I}(\vec{\kappa}' - \vec{\kappa}) \rangle_T \\
&+ \overline{N}^2 \langle \tilde{I}(-\vec{\kappa}) \tilde{I}(\vec{\kappa}) \rangle_T + \overline{N}^2 \langle \tilde{I}(\vec{\kappa}') \tilde{I}(-\vec{\kappa}') \rangle_T + \overline{N} \langle \tilde{I}(0) \rangle_T \} \\
&- \{ \overline{N}^3 \langle \tilde{I}(-\vec{\kappa}) \tilde{I}(\vec{\kappa}') \tilde{I}(\vec{\kappa} - \vec{\kappa}') \rangle_T + \overline{N}^2 \langle \tilde{I}(\vec{\kappa}' - \vec{\kappa}) \tilde{I}(\vec{\kappa} - \vec{\kappa}') \rangle_T
\end{aligned}$$

$$\begin{aligned}
& + \bar{N}^2 \langle \tilde{I}(-\vec{\kappa}') \tilde{I}(\vec{\kappa}') \rangle_{\tau} + \bar{N}^2 \langle \tilde{I}(\vec{\kappa}) \tilde{I}(-\vec{\kappa}) \rangle_{\tau} + \bar{N} \langle \tilde{I}(0) \rangle_{\tau} \} \\
& + \{ \bar{N}^2 \langle \tilde{I}(\vec{\kappa}' - \vec{\kappa}) \tilde{I}(\vec{\kappa} - \vec{\kappa}') \rangle_{\tau} + \bar{N} \langle \tilde{I}(0) \rangle_{\tau} \} . \quad (128)
\end{aligned}$$

Cancelling terms as appropriate, this expression can be reduced to the form

$$\begin{aligned}
\langle |S(\vec{\kappa}, \vec{\kappa}')|^2 \rangle &= \bar{N}^4 \langle \tilde{I}(-\vec{\kappa}') \tilde{I}(\vec{\kappa}') \tilde{I}(-\vec{\kappa}) \tilde{I}(\vec{\kappa}) \rangle_{\tau} \\
&+ \bar{N}^3 \langle \tilde{I}(0) \tilde{I}(-\vec{\kappa}) \tilde{I}(\vec{\kappa}) \rangle_{\tau} + \bar{N}^3 \langle \tilde{I}(-\vec{\kappa}' - \vec{\kappa}) \tilde{I}(\vec{\kappa}') \tilde{I}(\vec{\kappa}) \rangle_{\tau} \\
&+ \bar{N}^3 \langle \tilde{I}(\vec{\kappa}' + \vec{\kappa}) \tilde{I}(-\vec{\kappa}') \tilde{I}(-\vec{\kappa}) \rangle_{\tau} + \bar{N}^3 \langle \tilde{I}(0) \tilde{I}(-\vec{\kappa}') \tilde{I}(\vec{\kappa}') \rangle_{\tau} \\
&+ \bar{N}^2 \langle \tilde{I}(0) \tilde{I}(0) \rangle_{\tau} + \bar{N}^2 \langle \tilde{I}(-\vec{\kappa}' - \vec{\kappa}) \tilde{I}(\vec{\kappa}' + \vec{\kappa}) \rangle_{\tau} . \quad (129)
\end{aligned}$$

Now making use of Eq. (7) and removing from inside the angle brackets all the factors which do not depend in a statistical way on the turbulence induced wavefront distortion, as well as using Eq. 's (56) and (57), we can rewrite Eq. (129) as

$$\begin{aligned}
\langle |S(\vec{\kappa}, \vec{\kappa}')|^2 \rangle &= \bar{N}^4 |\tilde{I}_0(\vec{\kappa})|^2 |\tilde{I}_0(\vec{\kappa}')|^2 \langle |\tau(\vec{\kappa})|^2 |\tau(\vec{\kappa}')|^2 \rangle \\
&+ \bar{N}^3 [\tilde{I}_0(0) |\tilde{I}_0(\vec{\kappa})|^2 \langle \tau(0) |\tau(\vec{\kappa})|^2 \rangle_{\tau} + \tilde{I}_0^*(\vec{\kappa} + \vec{\kappa}') \tilde{I}_0(\vec{\kappa}') \tilde{I}_0(\vec{\kappa}) \langle \tau^*(\vec{\kappa} + \vec{\kappa}') \tau(\vec{\kappa}') \tau(\vec{\kappa}) \rangle_{\tau} \\
&+ \tilde{I}_0(\vec{\kappa} + \vec{\kappa}') \tilde{I}_0^*(\vec{\kappa}') \tilde{I}_0^*(\vec{\kappa}) \langle \tau(\vec{\kappa} + \vec{\kappa}') \tau^*(\vec{\kappa}') \tau^*(\vec{\kappa}) \rangle_{\tau} \\
&+ \tilde{I}_0(0) |\tilde{I}(\vec{\kappa})|^2 \langle \tau(0) |\tau(\vec{\kappa}')|^2 \rangle_{\tau} \} \\
&+ \bar{N}^2 \{ |\tilde{I}_0(0)|^2 \langle |\tau(0)|^2 \rangle_{\tau} + |\tilde{I}_0(\vec{\kappa} + \vec{\kappa}')|^2 \langle |\tau(\vec{\kappa} + \vec{\kappa}')|^2 \rangle_{\tau} \} . \quad (130)
\end{aligned}$$

Taking advantage of the fact that $\tilde{I}_0(0)$ and $\tau(0)$ are each equal to unity, this can be further reduced to yield the result that

$$\begin{aligned}
\langle |S(\vec{r}, \vec{r}')|^2 \rangle &= \bar{N}^4 |\tilde{I}_0(\vec{r})|^2 |\tilde{I}_0(\vec{r}')|^2 \langle |\tau(\vec{r})|^2 |\tau(\vec{r}')|^2 \rangle \\
&+ \bar{N}^3 \{ |\tilde{I}_0(\vec{r})|^2 \langle |\tau(\vec{r})|^2 \rangle_\tau + \tilde{I}_0^*(\vec{r} + \vec{r}') \tilde{I}_0(\vec{r}) \tilde{I}_0(\vec{r}') \langle \tau^*(\vec{r} + \vec{r}') \tau(\vec{r}) \tau(\vec{r}') \rangle_\tau \\
&+ \tilde{I}_0(\vec{r} + \vec{r}') \tilde{I}_0^*(\vec{r}) \tilde{I}_0^*(\vec{r}') \langle \tau(\vec{r} + \vec{r}') \tau^*(\vec{r}) \tau^*(\vec{r}') \rangle_\tau \\
&+ |\tilde{I}_0(\vec{r}')|^2 \langle |\tau(\vec{r}')|^2 \rangle_\tau \} \\
&+ \bar{N}^2 \{ 1 + |\tilde{I}_0(\vec{r} + \vec{r}')|^2 \langle |\tau(\vec{r} + \vec{r}')|^2 \rangle_\tau \} .
\end{aligned} \tag{131}$$

From Eq. (64) we see that we can write

$$|\langle S(\vec{r}, \vec{r}') \rangle|^2 = \bar{N}^4 |\tilde{I}_0(\vec{r})|^2 |\tilde{I}_0(\vec{r}')|^2 |\langle \tau^*(\vec{r}') \tau(\vec{r}) \rangle|^2 . \tag{132}$$

Making use of Eq. (74) we can rewrite this as

$$|\langle S(\vec{r}, \vec{r}') \rangle|^2 = \bar{N}^4 |\tilde{I}_0(\vec{r})|^2 |\tilde{I}_0(\vec{r}')|^2 (0.435)^2 (r_0/D)^4 \tau_{0L}(\vec{r}) \tau_{0L}(\vec{r}') . \tag{133}$$

Similarly making use of Eq. 's (74), (77), and (81) along with Eq. (131) we can write

$$\begin{aligned}
\langle |S(\vec{r}, \vec{r}')|^2 \rangle - |\langle S(\vec{r}, \vec{r}') \rangle|^2 &= \bar{N}^4 |\tilde{I}_0(\vec{r})|^2 |\tilde{I}_0(\vec{r}')|^2 (0.435)^2 (r_0/D)^4 \\
&\times \tau_{0L}(\vec{r}) \tau_{0L}(\vec{r}') \exp\{-6.88 [|\vec{r}' - \vec{r}| / (kr_0)]^{5/3}\} \\
&+ \bar{N}^3 \{ |\tilde{I}_0(\vec{r})|^2 (0.435) (r_0/D)^2 \tau_{0L}(\vec{r}) + |\tilde{I}_0(\vec{r}')|^2 (0.435) (r_0/D)^2 \tau_{0L}(\vec{r}') \}
\end{aligned}$$

$$+ \bar{N}^2 \{ 1 + |\tilde{I}_0(\bar{\kappa} + \bar{\kappa}')|^2 (0.435) (r_0/D)^2 \tau_{DL}(\bar{\kappa} + \bar{\kappa}') \} . \quad (134)$$

Substituting Eq.'s (133) and (134) into Eq. (125) and agreeing to restrict attention to values of $\bar{\kappa}$ and $\bar{\kappa}'$ sufficiently close together that we may approximate

$$\tau_{DL}(\bar{\kappa}) \approx \tau_{DL}(\bar{\kappa}') , \quad (135)$$

and for a nominally smooth image spectrum

$$\tilde{I}_0(\bar{\kappa}) \approx \tilde{I}_0(\bar{\kappa}') , \quad (136)$$

we get

$$\begin{aligned} \sigma_{\Delta\varphi}^2(\bar{\kappa}) = & (2M)^{-1} \{ \exp\{-6.88[\bar{\kappa}' - \bar{\kappa}]/(kr_0)]^{5/3}\} \\ & + 2[\bar{N} |\tilde{I}_0(\bar{\kappa})|^2 (0.435) (r_0/D)^2 \tau_{DL}(\bar{\kappa})]^{-1} \\ & + [\bar{N} |\tilde{I}_0(\bar{\kappa})|^2 (0.435) (r_0/D)^2 \tau_{DL}(\bar{\kappa})]^{-2} \\ & + \tilde{I}_0(\bar{\kappa} + \bar{\kappa}') \tau_{DL}(\bar{\kappa} + \bar{\kappa}') [\bar{N} |\tilde{I}_0(\bar{\kappa})|^4 (0.435) (r_0/D)^2 |\tau_{DL}(\bar{\kappa})|^2]^{-1} \} . \end{aligned} \quad (137)$$

Based on the assumption that $\bar{\kappa}$ and $\bar{\kappa}'$ are close enough that

$$6.88[\bar{\kappa} - \bar{\kappa}']/(kr_0)]^{5/3} \ll 1 , \quad (138)$$

it is reasonable to approximate Eq. (137) as

$$\sigma_{\Delta\phi}^2(\vec{\kappa}) \approx (2M)^{-1} \{1 + [\bar{N} |\tilde{I}_0(\vec{\kappa})|^2 (0.435)(r_0/D)^2 \tau_{0L}(\vec{\kappa})]^{-1}\}^2 . \quad (139)$$

The detected photon flux requirement for this result not to be photon shot-noise limited is that

$$\bar{N} \gg [|\tilde{I}_0(\vec{\kappa})|^2 (0.435)(r_0/D)^2 \tau_{0L}(\vec{\kappa})] . \quad (140)$$

Clearly, as we direct our attention to higher and higher spatial frequencies where $\tau_{0L}(\vec{\kappa})$ is smaller and smaller, and where presumably so is the image spectrum we require a higher and higher detected photon flux for our results to not be photon shot-noise limited. No matter what the photon flux rate, at some spatial frequency performance will become shot noise limited.

With Eq. (139) in hand we may now turn to our ultimate task, the evaluation of the resolution associated with the Knox-Thompson speckle imagery technique for a finite set of short exposures. We take this up in the next section.

3.12 Speckle Imagery Resolution

The basic equations for evaluation of the achievable resolution in speckle imagery are Eq. 's (123), (124), and (140) . In addition to these, we need expressions for \mathfrak{N} and some indication of how $\tilde{I}_0(\vec{\kappa})$ and $\tau_{DL}(\vec{\kappa})$ may be expected to vary as a function of $\vec{\kappa}$. We may approximate the form of $\tau_{DL}(\vec{\kappa})$ by the expression

$$\tau_{DL}(\vec{\kappa}) \approx 1 - 1.25 [|\vec{\kappa}|/(kD)] + 0.25 [|\vec{\kappa}|/(kD)]^4 , \quad (141)$$

where $k = 2\pi/\lambda$ and D is the telescope aperture diameter. As a practical matter, over most of the spatial frequency range of interest we may simply write

$$\tau_{DL}(\vec{\kappa}) \approx 0.5 , \quad (142)$$

as a sufficiently good approximation for our purposes.

If the object being viewed has an angular extent Θ_0 , and is reasonably "isotropic" in its size and complexity, and is complex in appearance (i.e., contains many features of all sizes), then it is probably reasonable to approximate

$$|\tilde{I}_0(\vec{\kappa})|^2 = [1 + (|\vec{\kappa}|/\kappa_0)^2]^{-1} , \quad (143)$$

where

$$\kappa_0 = \pi/\Theta_0 . \quad (144)$$

For the spatial frequencies of interest we can approximate

$$|\tilde{I}_0(\vec{\kappa})|^2 \approx (\kappa_0/|\vec{\kappa}|)^2 \quad . \quad (145)$$

To estimate \mathfrak{N} it is convenient to introduce the factor β relating the spatial frequency increment, i. e., $|\vec{\kappa} - \vec{\kappa}'|$, in our speckle imagery process to κr_0 . If the object size, Θ_0 , is small enough so that the turbulence limit sets the apparent image size and the extent of each of the recorded speckle patterns, then we know from analysis of the Knox-Thompson algorithm that we must use a spatial frequency separation such that

$$|\vec{\kappa} - \vec{\kappa}'| \leq \mu \kappa r_0 \quad , \quad (146)$$

where μ is a number less than one-half but probably greater than one-tenth. Nominally we take $\mu = 0.25$ for this analysis. If, however, Θ_0 is large enough so that the objects actual size sets the extent of the individual speckle patterns, so that it is ν^{-1} times as large as it would be for a purely turbulence limited extent, (where ν is a number less than unity), then the lowest spatial frequencies of interest would be of the order of

$$\begin{aligned} \kappa_0 &= \pi/\Theta_0 \\ &= \frac{1}{2} \nu \kappa r_0 \quad . \end{aligned} \quad (147)$$

Thus we may approximate

$$\beta = \begin{cases} \frac{1}{2} \nu , & \text{for } \Theta_0 > \lambda/r_0 \\ \mu , & \text{for } \Theta_0 < \lambda/r_0 \end{cases} \quad , \quad (148)$$

and write

$$|\vec{\kappa} - \vec{\kappa}'| = \beta k r_0 . \quad (149)$$

In estimating the image phase error at spatial frequency $\vec{\kappa}$ we shall make the convenient assumption that we are not going to bother to obtain data for spatial frequencies whose magnitude is greater than $|\vec{\kappa}|$. Accordingly, there will be

$$\mathcal{N} = \pi \beta^{-2} [|\vec{\kappa}|/(k r_0)]^2 . \quad (150)$$

It is convenient to note that in general we may consider $|\vec{\kappa}|$ to be a significant fraction of the optics spatial frequency cutoff, kD , i.e.,

$$|\vec{\kappa}| \approx \alpha k D , \quad (151)$$

where α is a number nominally between one-tenth and unity. Accordingly, we may rewrite Eq. (150) as

$$\mathcal{N} = \pi (\alpha/\beta)^2 (D/r_0)^2 . \quad (152)$$

Thus, we may recast Eq. (123) in the form

$$\sigma_{\Phi}^2 \approx \frac{2}{3} \left[\frac{4}{3} + \frac{1}{2} \ln (\alpha/\beta) + \frac{1}{2} \ln (D/r_0) \right] \sigma_{\Delta\Phi}^2 . \quad (153)$$

In general, we may expect the quantity in the square brackets to be dominated by the D/r_0 dependent term, so that we can approximate

$$\sigma_{\Phi}^2 \approx \left[\frac{1}{3} \ln (D/r_0) \right] \sigma_{\Delta\Phi}^2 . \quad (154)$$

It is obvious that the D/r_0 dependence, while not actually negligible will have only a minor impact on the overall phase error, σ_φ^2 . Doubling the telescope aperture diameter may effect σ_φ^2 through its effect on $\sigma_{\Delta\varphi}^2$, but will have only a very slight effect on σ_φ^2 through the $\ln(D/r_0)$ -term.

To evaluate $\sigma_{\Delta\varphi}^2$ we substitute Eq. (145) into Eq. (139). This allows us to write

$$\sigma_{\Delta\varphi}^2(\vec{\kappa}) \approx (2M)^{-1} \{1 + [0.435 \bar{N} (r_0/D)^2 (\kappa_0/|\vec{\kappa}|)^2 \tau_{BL}(\vec{\kappa})]^{-1}\}^2. \quad (155)$$

Making use of Eq. 's (142), (144), and (151) we can reduce this expression to the form

$$\begin{aligned} \sigma_{\Delta\varphi}^2(\vec{\kappa}) &\approx (2M)^{-1} \left\{ 1 + \{0.435 \bar{N} (r_0/D)^2 [(\pi/\theta_0)/(\alpha k D)]^2 (\frac{1}{2})\}^{-1} \right\}^2 \\ &\approx (2M)^{-1} \left\{ 1 + \{0.05 \alpha^{-2} (r_0/D)^2 [(\frac{\lambda/D}{\theta_0})^2 \bar{N}]^{-1}\}^{-1} \right\}^2 \end{aligned} \quad (156)$$

The quantity $[(\lambda/D)/\theta]^2$ can be considered to be the number of resolution elements in the target object (whether or not the target is greater than or smaller than λ/r_0), and so the quantity in the square brackets in Eq. (156) can be considered to be the number of detected photon events per exposure time per resolution element. It is this rather than any other measure of the total target brightness that determines whether or not the speckle imagery process is or is not limited by shot noise effects. The basic criteria for the process not to be shot noise limited is that

$$\bar{N} \left(\frac{\lambda/D}{\theta_0} \right) > 20 \alpha^2 (D/r_0)^2. \quad (157)$$

Since \bar{N} will only increase as D^2 , it follows from Eq. (155) that the larger the aperture diameter the brighter the target object has to be to yield a speckle imagery result that is not limited by photon shot noise.

If the target object is sufficiently bright that $\sigma_{\Delta\varphi}^2$ is essentially independent of \bar{N} , then the mean square phase error in the reconstructed target image using speckle imagery techniques is, in accordance with Eq. 's (154) and (156),

$$\sigma_{\varphi}^2 = \frac{\ln(D/r_0)}{6M}, \quad (158)$$

and the associated resolution is, in accordance with Eq. (124)

$$R_{s1} = (r_0/D)^{(1/8M)}. \quad (159)$$

When the target brightness is small enough that photon shot noise effects are significant, then we can write

$$\sigma_{\varphi}^2 = \left(\frac{(1+\gamma^{-1})^2}{2M} \right) \ln(D/r_0), \quad (160)$$

where

$$\gamma = \left[\frac{\bar{N}/(\frac{1}{4}\pi\theta_0^2)}{\frac{1}{4}\pi D^2} \right] \left[20 \left(\frac{\alpha}{\lambda} \right)^2 \left(\frac{D}{r_0} \right)^2 \right]^{-1}. \quad (161)$$

We note that γ is a measure of the target brightness, (corresponding to the first square bracket quantity) relative to the brightness required so that the speckle imagery process of the spatial frequency $|\vec{k}| = \alpha k D$ will not be limited by shot noise effects. It is interesting to note that this required brightness level is independent of aperture diameter, D ,

if we hold the spatial frequency, $|\vec{\kappa}|$, constant, but increases with D^2 if we ask that the spatial frequency always be a constant fraction of the aperture cutoff frequency, kD — i. e., if we hold α constant as we vary D .

Substituting Eq. (154) into Eq. (124) we obtain as our final result the expression

$$R_{s1} = (r_0/D)(1+\gamma^{-1})^2 / (6M) \quad , \quad (162)$$

the speckle imagery resolution. This represents the last of the results we undertook to develop in this chapter.

3.13 References for Chapter 3

- 1a. A. Labeyrie, Astr. and Ap. 6, 85 (1970).
- 1b. A. Labeyrie, "High Resolution Techniques in Optical Astronomy," in Progress in Optics Vol XV, E. Wolf, ed., (North Holland, Amsterdam 1976).
2. K. T. Knox and B. J. Thompson, "Recovery of Images from Atmospherically Degraded Short-Exposure Photographs," Ap. J. 193, L45 (1974) .
3. D. L. Fried, "Statistics of a Geometric Representation of Wavefront Distortion," J. Opt. Soc. Am., 55 , 1427 (1965).
4. D. L. Fried, "Optical Heterodyne Detection of an Atmospherically Distorted Signal Wavefront," Proc. IEEE 55, 57 (1967).
5. D. L. Fried, "Optical Resolution Through a Randomly Inhomogeneous Medium for Very Long and Very Short Exposures," J. Opt. Soc. Am. 56, 1372 (1966).
6. F. Roddier, "Signal-to-Noise Ratio in Speckle Interferometry," in Imaging in Astronomy, Technical Digest, AAS/SAO/OSA/SPIE Topical Meeting June 18-21, 1975, Cambridge, MA.
- 7a. J. C. Dainty, "Stellar Speckle Interferometry," in Laser Speckle and Related Phenomena (Topics in Applied Physics, Vol 9), J. C. Dainty, ed., (Springer, Berlin 1975).
- 7b. J. C. Dainty, "The Signal-to-Noise Ratio in Speckle Interferometry," in High Angular Resolution Stellar Interferometry: The Proceedings of Colloquium No. 50 International Astronomical Union, held at the Univ. of Maryland, College Park, MD, 30 Aug - (Chatterton Astronomy Dept., Univ of Sidney, NSW 2006 Australia, 1979.)
8. R. K. Luncburg, Mathematical Theory of Optics (Advanced Instruction and Research in Mechanics; Summer, 1944), (Brown Univ., Providence 1944).

9. D. Korff, "Analysis of a Method of Obtaining Near-Diffraction-Limited Information in the Presence of Atmospheric Turbulence," J. Opt. Soc. Am. 63, 971 (1973).
10. D. L. Fried, "Angular Dependence of Atmospheric Turbulence Effects in Speckle Interferometry," in High Angular Resolution Stellar Interferometry: The Proceedings of Colloquium No. 50 International Astronomical Union, held at the Univ. of Maryland, College Park, MD, 30 Aug - 15 Sep 1978. (Chatterton Astronomy Dept., Univ. of Sidney, NSW 2006 Australia, 1979).
11. D. L. Fried, "Least-Square Fitting a Wavefront Distortion Estimate to an Array of Phase-Difference Measurements," J. Opt. Soc. Am. 67, 370 (1977).

END